Neurobiology of Disease 218 (2026) 107205

Contents lists available at ScienceDirect

Neurobiology of Disease

journal homepage: www.elsevier.com/locate/ynbdi

Modeling Mowat-Wilson syndrome with patient iPSCs reveals transcriptional and phenotypic defects in neural progenitors

Ilaria Musante [a], Giulia Gorrieri [a], Serena Tamburro [b], Giulia Ferrera [c,d], Simona Baldassari [a], Anna Fetta [e,f], Stefano Giuseppe Caraffi [g], Aglaia Vignoli [d,h], Giovanni Fiorito [i], Livia Garavelli [g], Maria Paola Canevini [c,d], Duccio Maria Cordelli [e,f], Federico Zara [a,b], Emilia Ricci [c,d,**], Paolo Scudieri [a,b,*]

[a] Medical Genetics Unit, IRCCS Istituto Giannina Gaslini, Genoa, Italy
[b] Department of Neurosciences, Rehabilitation, Ophthalmology, Genetics, Maternal and Child Health (DiNOGMI), University of Genoa, Genoa, Italy
[c] Child Neurology Unit-Epilepsy Center, San Paolo Hospital, Member of ERN-Epicare, Milan, Italy
[d] Department of Health Sciences, University of Milan, Milan, Italy
[e] U.O.C. Neuropsichiatria dell'età Pediatrica, IRCCS Istituto delle Scienze Neurologiche di Bologna, Bologna, Italy
[f] Dipartimento di Scienze Mediche e Chirurgiche (DIMEC), Alma Mater Studiorum, Università di Bologna, Bologna, Italy
[g] SOC Genetica Medica, Azienda USL-IRCCS di Reggio Emilia, Reggio Emilia, Italy
[h] Childhood Neurology and Psychiatry Unit, Azienda Socio Sanitaria Territoriale Grande Ospedale Metropolitano (ASST GOM) Niguarda, Milan, Italy
[i] Clinical Bioinformatics Unit, IRCCS Istituto Giannina Gaslini, Genoa, Italy

ARTICLE INFO

Keywords:
Disease models
Pluripotent stem cells
Neural induction
Cell motility

ABSTRACT

Zinc finger *E*-box-binding homeobox 2 (*ZEB2*) is a key transcription factor involved in multiple aspects of nervous system development, including neuronal specification, migration, and differentiation. Loss-of-function variants in *ZEB2* cause Mowat-Wilson syndrome (MWS), a severe neurodevelopmental disorder characterized by intellectual disability, epilepsy, and brain structural abnormalities. In this study, we generated and characterized induced pluripotent stem cell (iPSC) lines from MWS patients carrying pathogenic *ZEB2* variants. Patient-derived iPSCs retained full pluripotency and were capable of differentiating into all three germ layers, including neural lineages. Upon directed differentiation into neural progenitor cells (NPCs) and early neurons, we identified distinctive transcriptional alterations affecting neuroepithelial-to-radial glia transition and lineage specification. RNA-seq analysis revealed dysregulation of genes involved in cytoskeletal remodeling, extracellular matrix organization, and cell motility. Functional holographic live imaging confirmed a significant increase in motility behavior in MWS NPCs and early neurons, suggesting that altered cell dynamics may underlie aberrant neural circuit formation. Despite these changes, early neuronal markers such as MAP2 were expressed at comparable levels in MWS and control cells. Together, these findings uncover novel cellular and molecular phenotypes associated with *ZEB2* deficiency and provide insight into how disrupted progenitor behavior and transcriptional mis-regulation may contribute to the neurodevelopmental features of MWS.

1. Introduction

Zinc finger *E*-box-binding homeobox 2 (*ZEB2*), also known as SIP1 or ZFHX1B, encodes a transcription factor essential for multiple aspects of nervous system development, including progenitor cell fate specification, neuronal migration, and differentiation (Epifanova et al., 2019). While *ZEB2* primarily functions as a transcriptional repressor, it can also act as an activator depending on the cellular context and availability of specific cofactors (Epifanova et al., 2019). Its widespread expression is critical for the proper formation of both central and peripheral nervous system structures (Epifanova et al., 2019).

Germline haploinsufficiency of *ZEB2* causes Mowat-Wilson syndrome (MWS, MIM #235730), a rare congenital neurodevelopmental disorder characterized by facial dysmorphisms, agenesis/hypoplasia of

* Correspondence to: P. Scudieri, Medical Genetics Unit, IRCCS Istituto Giannina Gaslini, Genoa, Italy.
** Correspondence to: E. Ricci, Child Neurology Unit-Epilepsy Center, San Paolo Hospital, Member of ERN-Epicare, Milan, Italy.
E-mail addresses: emilia.ricci@asst-santipaolocarlo.it (E. Ricci), paolo.scudieri@unige.it (P. Scudieri).

https://doi.org/10.1016/j.nbd.2025.107205
Received 8 September 2025; Received in revised form 26 November 2025; Accepted 27 November 2025
Available online 29 November 2025

Table 1
Clinical details of MWS individuals selected for the generation of iPSC lines.

Patient ID	Sex (M/F)	Age at last follow up (years, months)	Growth parameters at birth// at last FU (percentile, SD)	Facial phenotype	Behavioral phenotype	Other clinical characteristics	Neurological examination at last follow up	Epilepsy (yes/no); age at onset (years, months)	Seizures types	EEG features at last follow up	MRI findings	ZEB2 pathogenic variant (cDNA, NM_014795.4; protein, NP_055610.1)
GGB11415F; previously published in (Cordelli et al., 2013) (pt 2); (Garavelli et al., 2017; Ivanovski et al., 2018) (pt 19); (Ricci et al., 2021) (pt 15), (Caraffi et al., 2024) (pt 18)	F	6	*W*: 30, −0.5 *H:* 58, +0.2 *HC:* 11, −1.2 // *W*: 57, +0.2 *H:* 73, +0.6 *HC*: 7, −1.5	Uplifted ear lobes, central depression of ear lobes, rounded skull, sparse hair, fine hair, large eyes, deep-set eyes, hypertelorism, telecanthus, broad nasal bridge, prominent columella, open mouth, M-shaped upper limb,	Frequent smiling, chewing/ mouthing objects or body parts, eating non-food items, grinding teeth, under-reaction to pain, rapid mood changes,	Slender, tapering fingers, long toes, genu valgus, broad, long halluces, overriding of toes, widely spaced teeth, delayed tooth eruption	Severe intellectual delay, motor stereotypies	Yes; 2,6	Focal, atypical absence	Slowing of background activity, fronto-central R spikes, occipital spikes	Partial agenesis of CC, dysmorphic hippocampal	c.2682del; p.(Leu894Phefs*36)
GGB28215F previously published in (Cordelli et al., 2013) (pt 19); (Ivanovski et al., 2018) (pt 62); (Ricci et al., 2021) (pt 17), (Caraffi et al., 2024) (pt 22)	F	15,2	*W*: 48, 00 *H:* na *HC*: na // *W:* 60, +0.3 *H*: 18, −0.9 *HC:* 1, −2.4	Microcephaly, large eyebrows, medially flaring eyebrows, sparse eyebrows in the middle, uplifted ear lobes, central depression of the ear lobes, rounded skull, fine hair, high forehead, large eyes, telecanthus, hypertelorism depressed nasal bridge, prominent columella, open mouth, M-shaped upper lip, elongation of the face depression of the nasal tip prognathism,	Frequent smiling, chewing/ mouthing object or body parts, grinding teeth, flickering/ tapening/ twirling objects, repetitive activities, standing too close to others, under-reaction to pain, excessive elation, rapid mood changes, laughing with no reason	Constipation, patent ductus arteriosus, ventricular septal defect, atrial septal defect, prominence of interphalangeal joints, astigmatism, widely spaced teeth, palmar and plantar creases, recurrent otitis media or other infections	Severe intellectual delay, motor stereotypies	Yes; 0,1	Focal, atypical absence, status epilepticus	Slowing of background activity, diffuse frontal dominant high voltage slow waves	Complete agenesis of CC, lateral ventricle enlargement	c.650_653dup; p.(Gly219Profs*21)
GGB11515M previously published in (Garavelli et al., 2017; Ivanovski et al., 2018) (pt 27); (Caraffi et al., 2024) (pt 19)	M	5, 11	*W*: 22, −0.8 *H:* 33, −0.4 *HC:* 15, −1 // *W*: 3, −2.0 *H*: 20, −0.9 *HC:* <1, −2.9	Microcephaly, sparse eyebrows in the middle, uplifted ear lobes, rounded skull, fine hair, high forehead, frontal bossing, large eyes, epicanthal folds, hypertelorism, telecanthus, broad nasal bridge, depressed nasal bridge, rounded nasal tip, prominent	Frequent smiling, chewing/ mouthing objects or body parts, flickering / tapening / twirling objects, grinding teeth, repetitive activity, under-reaction to pain, excessive elation,	Hirschsprung disease, Pyloric stenosis, patent ductus arteriosus, cryptorchidism, slender and tapering fingers, mild calcaneovalgus, pectus excavatum, superior pectus carinatum/ inferior pectus excavatum, adducted thumbs, hallux valgus, hypoplasia of toes middle and distal	Hypotonia, severe intellectual delay, motor stereotypies	Yes, 3	Focal, focal to bilateral tonic-clonic seizure	na	Partial agenesis of CC, ventricular temporal horn enlargement, reduction of thickness of WM	c.817del; p.(Leu273*)

(*continued on next page*)

Table 1 (*continued*)

Patient ID	Sex (M/F)	Age at last follow up (years, months)	Growth parameters at birth// at last FU (percentile, SD)	Facial phenotype	Behavioral phenotype	Other clinical characteristics	Neurological examination at last follow up	Epilepsy (yes/no); age at onset (years, months)	Seizures types	EEG features at last follow up	MRI findings	ZEB2 pathogenic variant (cDNA, NM_014795.4; protein, NP_055610.1)
				columella, open mouth, M-shaped upper lip, prominent chin	laughing with no reason	phalanges, overriding of the toes, strabismus, myopia, astigmatism, widely spaced teeth, recurrent otitis media or other infections						
GGB16117M previously published in (Ivanovski et al., 2018) (pt 89); (Caraffi et al., 2024) (pt 24)	M	4,10	*W:* 36, −0.4 *H:* 39, −0.3 *HC:* 20, −0.8 // *W:* 52, 0.0 *H:* 12, −1.2 *HC*: <1, −2.7	Microcephaly, large eyebrows, medially flaring eyebrows, sparse eyebrows in the middle, uplifted ear lobes, central depression of the ear lobes, frontal bossing, epicanthal folds, depressed nasal bridge, prominent columella, M-shaped upper lip, prominent chin	Frequent smiling, chewing / mouthing objects or body parts	Patent ductus arteriosus, pulmonary artery stenosis, ventricular septal defect, crossed pulmonary arteries, hypospadia, craniosynostosis (trigonocephaly), prominence of interphalangeal joints, pes planus, genu valgus, mild contractures of the hip/elbows/knees, broad halluces, hypermetropia, recurrent otitis media or other infections	severe intellectual delay	Yes; 3,6	Motor seizures not better defined (focal?)	na	Partial agenesis of CC	c.1578_1579delinsA; p.(Asp527Thrfs*17)

C = central; CC = corpus callosum; F = female; H = height; HC = head circumference; M = male; na = not available; O = occipital; R = right; W = weight; WM = white matter.

the corpus callosum, intellectual disability, and a high prevalence of epilepsy (75–85 % of individuals) (Mowat et al., 1998; Ivanovski et al., 2018; Cordelli et al., 2021). While early reports attributed epilepsy in MWS to structural brain anomalies (Engenheiro et al., 2008), more recent studies suggest also a genetically driven, cellular and circuit-level etiology. In a detailed electroclinical characterization, Ricci and colleagues described a stereotyped, age-dependent seizure progression (from febrile seizures in infancy to focal hypnic seizures and atypical absences, followed by remission in adolescence) with consistent responsiveness to valproate and no imaging findings typically associated with epileptogenic cortical malformation (Di Pisa et al., 2019; Ricci et al., 2021). These findings support the hypothesis that seizures in MWS also stem from more diffuse neurodevelopmental dysfunction. Interestingly, generalized epileptic discharges and absence seizures were frequently observed in patients with complete corpus callosum agenesis, suggesting that seizure propagation in MWS may involve cortical-subcortical circuits rather than interhemispheric pathways (Ricci et al., 2021). GABAergic inhibition has been proposed as a key regulator of such circuits, especially in seizure types like absence epilepsy (Galanopoulou, 2010; Miyamoto et al., 2019; Pfisterer et al., 2020). *ZEB2* has been shown to be crucial for the migration and fate specification of GABAergic interneurons derived from the medial ganglionic eminence (Epifanova et al., 2021; McKinsey et al., 2013; Takagi et al., 2015; van den Berghe et al., 2013). In mouse models, loss of *Zeb2* disrupts interneuron migration and alters their identity, leading to a shift from cortical to striatal fates and potentially contributing to excitation-inhibition imbalance (Epifanova et al., 2021; McKinsey et al., 2013; Takagi et al., 2015; Tomassy et al., 2013; van den Berghe et al., 2013). In addition to transcriptional dysregulation, abnormal neuronal morphology may also play a role in MWS epileptogenesis. *Zeb2* knockout mice display significantly shorter axons in cortical neurons compared to controls (Srivatsa et al., 2015), resembling defects reported in GABAergic neurons derived from SCN1A-mutated patients, which exhibit reduced dendritic arborization (Tiraboschi et al., 2020).

While these insights largely stem from animal models, patient-derived induced pluripotent stem cell (iPSCs) offer a unique and ethically feasible approach to study neural development and dysfunction in a human context. A pioneering iPSC-based study of *ZEB2* haploinsufficiency demonstrated impaired interneuron differentiation and altered gene expression (Schuster et al., 2022). However, due to the limited number of patient-derived lines available, further validation and expansion of these findings in additional models is needed to further elucidate the effects of *ZEB2* variants.

In this study, we sought to advance understanding of *ZEB2*-related neurodevelopmental dysfunction by generating and characterizing iPSC-derived neural progenitor cells (NPCs) from four unrelated individuals carrying pathogenic *ZEB2* variants. Transcriptomic profiling revealed dysregulation of genes involved in neuroepithelial-to-radial glia transition, lineage specification, cytoskeletal remodeling, and extracellular matrix interaction. In parallel, live-cell imaging demonstrated increased cell motility during early neuronal differentiation. Together, these findings provide novel molecular insights into *ZEB2*-associated neurodevelopmental dysfunction and reinforce the link between transcriptional dysregulation and epileptogenesis in MWS, thereby advancing our understanding of disease pathogenesis and identifying potential therapeutic targets.

2. Materials and methods

2.1. Cell reprogramming and culture conditions

Four MWS patients were selected for the generation of iPSC lines. Table 1 summarizes the clinical features of each individual with MWS. Peripheral blood mononuclear cells (PBMCs) were obtained from the Biobank of the Laboratory of Human Genetics – IRCCS Istituto Giannina Gaslini (a member of the Telethon Network of Genetic Biobanks, Project No. GTB18001) (Galliera Genetic Bank: A DNA and Cell Line Biobank from Patients Affected by Genetic Diseases, 2016). The following biobank ID numbers GGB11415F, GGB28215F, GGB11515M, and GGB16117M correspond to patients P1, P2, P3, and P4, respectively, in this study. As controls, we used two established iPSC lines derived from healthy individuals: C1 (female donor, age 1), originally described by Aprile et al., 2019 (Aprile et al., 2019), and C2 (male donor, age 1), a previously used and commercially available line (Musante et al., 2025).

Table 2
Primers used for Sanger sequencing and RT-PCR.

Target	Size (bp)	Forward and Reverse primer (5′-3′)
Primers for *ZEB2* variants validation		
c.2682del	234	AGATGAGCCTCTGAACTTGACT
		TGTGGTAGGAAGCTCATCTG
c.650_653dup	235	GCCCATTAGCTGCCATTGAT
		CGGTAGGCAAACGTGTAGC
c.817del	363	AGCATGCACTCAAACCTTTTG
		CAGGCACACAGAGTTGATGA
c.1578_1579delinsA	250	AGGATCCATGCTCTCAACCT
		ACTGGCATGAAAATGGAGTGG
Primers for RT-PCR of viral genes		
SeV	181	GGATCACTAGGTGATATCGAGC
		ACCAGACAAGAGTTTAAGAGATATGTATC
KOS	528	ATGCACCGCTACGACGTGAGCGC
		ACCTTGACAATCCTGATGTGG
Klf4	410	TTCCTGCATGCCAGAGGAGCCC
		AATGTATCGAAGGTGCTCA
c-Myc	532	TAACTGACTAGCAGGCTTGTCG
		TCCACATACAGTCCTGGATGATGATG
ATP5F1	575	TTAGCGCAGAGACCTTCACT
		CCAGTGCCTGTTGTGACTTC

For the reprogramming, PBMCs were thawed on day −4 and cultured at 37 °C with 5 % CO_2 in PBMC medium (StemPro™-34 SFM; 10,639,011, Thermo Fisher Scientific) supplemented with appropriate cytokines, following the recommendations of the Sendai viral transduction kit CytoTune-iPS 2.0 protocol (A1569601, Thermo Fisher Scientific). On the day of transduction, 3×10^5 PBMCs were counted and transduced with Sendai reprogramming vectors at MOI 5:5:3 (KOS, hc-Myc, hKlf4), following the manufacturer protocol (A1569601, Thermo Fisher Scientific). Briefly, cells and viruses were mixed in PBMC medium, centrifuged at 1000 ×*g* for 30 min at room temperature, and then transferred to one well of a 12-well plate. The plate was incubated overnight at 37 °C and 5 % CO_2. The following day, the medium containing viruses was removed by centrifuging the cell suspension at 200 ×*g* for 10 min. Cells were then resuspended in 0.5 ml of complete PBMC medium per well of a 24-well plate. At day 3 after transduction, 1×10^4 to 1×10^5 live cells were plated onto Geltrex™-coated (A1413302, Thermo Fisher Scientific) 6-well plates in 2 ml of PBMC medium without the cytokines. Every other day, half of the spent medium was gently removed and replaced with 1 ml of fresh StemPro™-34 medium without cytokines until day 7. At day 8, PBMC medium was replaced with Essential 8™ Medium (A1517001, Thermo Fisher Scientific) until iPSC colonies appeared. From day 15 post-transduction, colonies were ready for picking and were transferred into Geltrex-coated 12-well plates in Essential 8™ Medium, which was subsequently replaced with Essential 8™ Flex Medium (A2858501, Thermo Fisher Scientific). Colonies were cultured until passage 10 on Geltrex-coated 6-well plates in Essential 8™ Flex Medium at 37 °C with 5 % CO_2. Cells were passaged every 2–3 days at a ratio of 1:5 to 1:10 using Versene solution (15,040,066, Thermo Fisher Scientific). During passaging and thawing steps, the medium was supplemented overnight with RevitaCell™ (A2644501, Thermo Fisher Scientific) overnight. Cell freezing was performed using Bambanker (BB01, NIPPON Genetics EUROPE).

Table 3
Antibodies used for immunofluorescence.

Target	Catalog number	Dilution
OCT4	703,927, Thermo Fisher Scientific	1:500
SSEA-4	MA1–021, Thermo Fisher Scientific	1:500
TRA-1-60	MA1–023, ThermoFisher Scientific	1:250
SOX2	14–9811-82, Thermo Fisher Scientific	1:250
PAX6	MA1–109, Thermo Fisher Scientific	1:200
β3-tubulin	302,304, Synaptic Systems	1:200
TBXT	14–9770-82, Thermo Fisher Scientific	1:100
TBX6	BS-12281R, Thermo Fisher Scientific	1:100
SOX17	MA5–24885, Thermo Fisher Scientific	1:50
FOXA2	701,698, Thermo Fisher Scientific	1:100
SOX1	MA5–32447, Thermo Fisher Scientific	1:200
MAP2	188,004, Synaptic Systems	1:500

2.2. Genetic analysis of iPSC lines

The presence of the expected *ZEB2* variants in the newly generated iPSC lines was verified by Sanger sequencing, while array-CGH with the SurePrint G3 Human CGH Microarray Kit 180 K (G4449 A, Agilent) detected no chromosomal rearrangements. The complete array-CGH datasets will be made available upon request.

Genomic DNA was extracted from PBMCs and iPSCs using the QIAmp DNA micro kit (56,304, Qiagen). DNA concentration was measured with NanoDrop 1000 spectrophotometer (Thermo Fisher Scientific). 100 ng of total DNA was used to perform PCR using the AmpliTaq Gold™ 360 Master Mix. The sequences of forward and reverse primers used are listed in Table 2. The PCR products, purified using ExoSAP-IT (78,201, Applied Biosystems), were subjected to sequencing PCR with BigDye Terminator v1.1 Cycle Sequencing kit (4,336,774, Applied Biosystems), according to manufacturer's instructions. Then, capillary electrophoresis by ABI PRISM 310 Genetic Analyzer (Thermo Scientific) was performed to obtain sequences electropherograms.

2.3. Reverse transcription PCR (RT-PCR)

RT-PCR on iPSCs at passage 10 was performed to verify the loss of exogenous factor genes. For this purpose, RNA extraction was performed using RNeasy Mini Kit (74,104, Qiagen), according to the manufacturer's protocol. The RNA concentration was measured with NanoDrop 1000 spectrophotometer (Thermo Fisher Scientific). 250 ng of total RNA was used for cDNA synthesis with iScript™ cDNA Synthesis Kit (1,708,891, Biorad). cDNA was used to perform PCR using the AmpliTaq Gold™ 360 Master Mix (4,398,881, Thermo Fisher Scientific). PCR products were separated by electrophoresis on a 2 % agarose gel containing EuroSafe Nucleic Acid Stain (EMR440001, Euroclone) and visualized under UV illumination using a Mini HD9 system (Uvitec Cambridge). The sequences of forward and reverse primers used are listed in Table 2.

2.4. Trilineage differentiation

To assess pluripotency, iPSC lines were subjected to directed differentiation into mesoderm, endoderm, and ectoderm lineages using the STEMdiff™ Trilineage Differentiation Kit (05230, STEMCELL Technologies), according to the manufacturer's instructions. Briefly, iPSCs were plated onto Geltrex™-coated 8-chamber slides (80,841, IBIDI) and cultured in lineage-specific induction media. Endodermal and mesodermal differentiation was carried out over 5 consecutive days, while ectodermal differentiation was performed over 7 days, with daily medium changes for all conditions. At the end of the differentiation period, cells were fixed with 10 % neutral buffered formalin (05-01005Q, Bio-Optica) and subjected to immunofluorescence analysis using antibodies targeting lineage-specific markers for each germ layer, as described in the following section and listed in Table 3.

2.5. Generation of iPSC-derived neural progenitor cells (NPC)

iPSC-derived NPCs were generated via dual inhibition of SMAD signaling using the STEMdiff Neural System (STEMCELL Technologies), following the manufacturer's instructions and as previously described in (Musante et al., 2025). Briefly, iPSC colonies were detached by incubating with StemPro™ Accutase™ Cell Dissociation Reagent (A1110501, Thermo Fisher Scientific) for 5 min. The cells were then collected by gentle pipetting in DMEM/F12 medium (11,330,057, Thermo Fisher Scientific) to obtain a single-cell suspension. Following centrifugation at 300 $\times g$ for 5 min, the cells were resuspended in STEMdiff™ Neural Induction Medium + SMADi (08581, STEMCELL Technologies) supplemented with RevitaCell™ (A2644501, Thermo Fisher Scientific). A total of 3×10^6 cells were seeded into each well of an AggreWell™ 800 plate (34,811, STEMCELL Technologies) in a final volume of 2 ml. The plate was centrifuged at 100 $\times g$ for 3 min to facilitate cell capture in the microwells, and three-quarters of the medium was replaced daily for 5 days. During this period, iPSCs aggregated at the bottom of the wells to form embryoid bodies (EBs). These EBs were then collected and plated onto 6-well plates coated with Geltrex™ (A1413302, Thermo Fisher Scientific) and cultured for an additional 7 days to allow the formation of neural rosettes. Subsequently, neural rosettes were detached using STEMdiff™ Neural Rosette Selection Reagent (05832, STEMCELL Technologies) and transferred to a Geltrex-coated well of a 6-well plate. NPCs emerging from the neural rosettes were cultured for 5–7 days. To obtain a single-cell suspension, NPCs were dissociated using Accutase and transferred to a 6-well plate in STEMdiff™ Neural Progenitor Medium (05833, STEMCELL Technologies) at a density of 1×10^6 cells per well, defined as NPC passage 1. NPCs were expanded and maintained by feeding every other day with Neural Progenitor Medium.

2.6. Generation of NPC-derived early neurons

NPCs were plated in STEMdiff Neural Progenitor medium on Geltrex-coated 24-well plates (82,426, IBIDI) at a density of 4×10^4 cells/well. After 24 h, the medium was replaced with Neurobasal Medium (21,103,049, Thermo Fisher Scientific) supplemented with GlutaMax Supplement (1:100), B-27 supplement (1:50), BDNF (10 ng/ml), GDNF (10 ng/ml), retinoic acid (1 μM), ascorbic acid (200 μM) and CulturOne supplement (1:100). Half of the medium was replaced twice a week during continuous culturing. From day 5 (d5) onward, Neurobasal Medium and B-27 supplement were substituted by Neurobasal Plus Medium (A3582901, Thermo Fisher Scientific) and B-27 Plus supplement (A3582801, Thermo Fisher Scientific), respectively. Throughout the differentiation period, NPC-derived neurons were monitored using label-free holographic imaging and were fixed at day 10 (d10) with 10 % neutral buffered formalin for subsequent immunofluorescence analysis.

2.7. Immunofluorescence analysis

Control and MWS cells were subjected to immunofluorescence detection and quantification of specific markers to verify proper progression through key developmental stages: undifferentiated state (OCT4, SSEA-4, TRA-1-60, and SOX2) and pluripotency/trilineage differentiation (PAX6 and β3-tubulin for ectoderm, TBXT and TBX6 for mesoderm, and SOX17 and FOXA2 for endoderm) of iPSC lines, neural identity of iPSC-derived neural progenitor cells (SOX1 and PAX6), and early neuronal maturation (MAP2).

Cells were washed in PBS and fixed with 10 % neutral buffered formalin (05-01005Q, Bio-Optica) for 5 min at room temperature. After three washings in PBS, cells were permeabilized with Triton X-100 0.3 % in PBS for 5 min, blocked with 1 % BSA in PBS for 2 h, and then incubated overnight at 4 °C with a solution of primary antibodies diluted in PBS containing 1 % BSA. Antibody details, including catalog numbers and dilutions, are listed in Table 3. Following incubation with primary

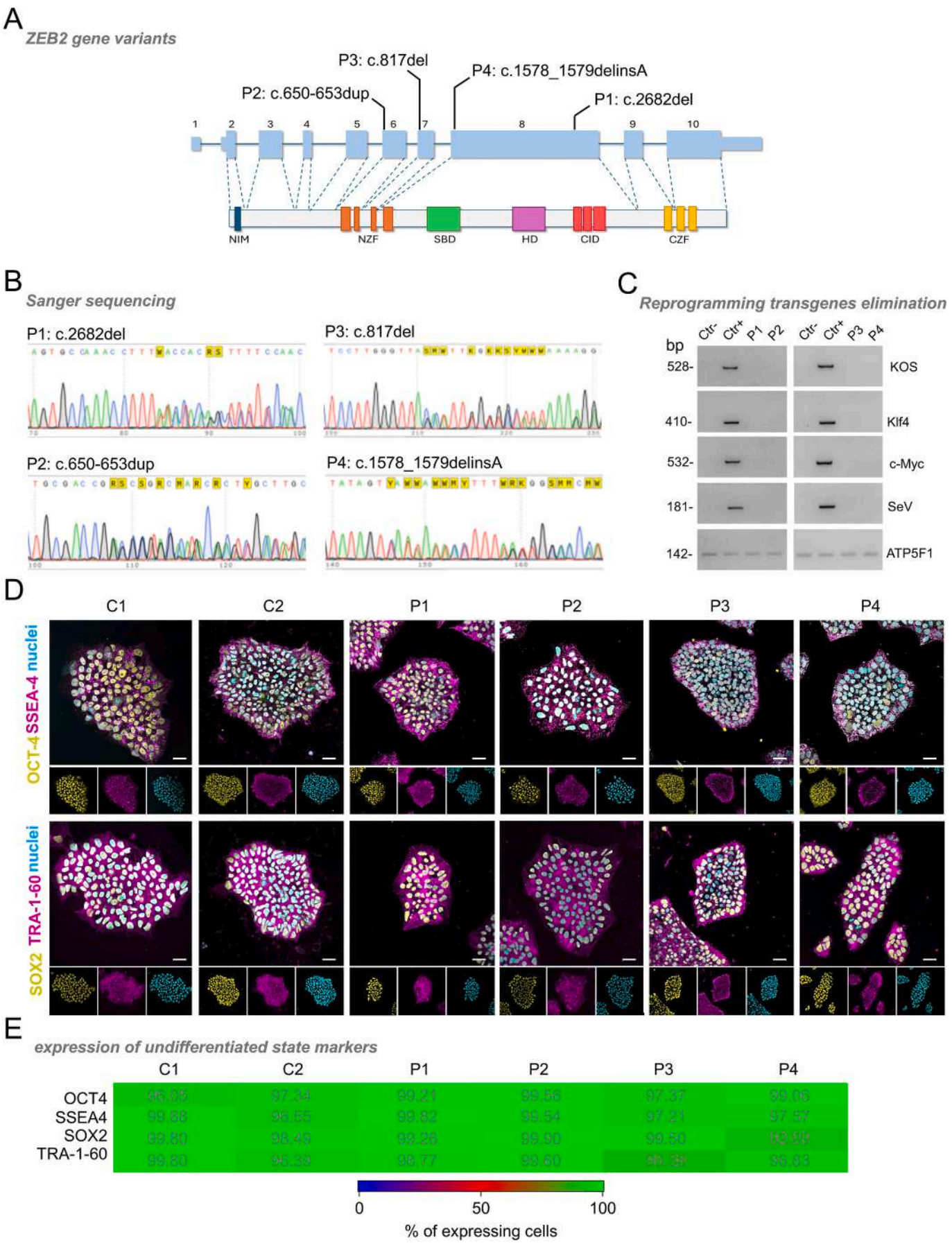

(caption on next page)

Fig. 1. Generation of MWS iPSCs carrying ZEB2 variants. (A) Schematic representation of the ZEB2 gene and its encoded protein. Positions of the mutations identified in patients P1–P4 are indicated. (B) Sanger sequencing traces confirming the presence of ZEB2 variants in the selected iPSC clones. (C) RT-PCR analysis showing the loss of exogenous viral gene expression. PCR products were separated by agarose gel electrophoresis. The first two lanes represent cDNA from PBMCs before (Ctr-) and after (Ctr+) delivery of reprogramming viruses. Lanes P1-P4 correspond to patient-derived iPSC clones at passage 10, which no longer express the reprogramming transgenes (KOS, Klf4, c-MYC, SeV). ATP5F1 was used as a housekeeping control. (D, E) Representative confocal images (D) and heatmap (E) showing the expression of undifferentiated state markers in control (C1, C2) and patient-derived iPSC lines. Immunofluorescence analysis was performed for OCT4, SSEA4, SOX2, and TRA-1–60. Scale bar: 25 μm. A total of $n = 2000$ cells were analyzed at the passage preceding cell banking and neural induction, with >90 % of cells expressing each marker (values indicated in heatmap).

antibodies, cells were rinsed three times in PBS and incubated with a solution of secondary Alexa Fluor–conjugated antibodies (Thermo Fisher Scientific) diluted 1:200 in PBS containing 1 % BSA for 1 h in the dark. After further three washes in PBS, the slides were mounted with Fluoroshield with DAPI to stain cell nuclei.

Image acquisition was performed using a laser scanning confocal microscope TCS SP8 (Leica Microsystems) and an Eclipse TiE automated microscope (Nikon) to acquire high-resolution representative images and for quantitative analysis, respectively. Image analysis was performed using the General Analysis package in NIS Elements AR software as detailed in Musante et al., 2025 (Musante et al., 2025). Nuclear morphology was assessed on DAPI-stained images by measuring nuclear area and circularity using the same software package.

2.8. QuantSeq 3′ mRNA sequencing library preparation

Transcriptomic analysis was performed on 4 separate preparations of NPCs derived from MWS-iPSC lines (P1-P4) and two control iPSC lines (C1, C2). Total RNA was extracted using the RNeasy Mini Kit (74,104, Qiagen), following the manufacturer's protocol. RNA concentration was quantified using the Qubit 4.0 Fluorometer (Thermo Fisher Scientific) and adjusted to 10 ng/μL.

Libraries were prepared from 125 ng of total RNA using the NEGEDIA Digital mRNA-seq research grade sequencing service v2.0 (Next Generation Diagnostic srl) which included library preparation, quality assessment, and sequencing. Sequencing was performed on a NovaSeq 6000 system (Illumina Inc.) using a single-end, 100-cycle strategy.

2.9. QuantSeq 3′ mRNA sequencing data processing and analysis

Raw sequencing data were analyzed using the proprietary NEGEDIA Digital mRNA-seq pipeline (v2.0) provided by Next Generation Diagnostic srl. The pipeline includes quality filtering and trimming, alignment to the reference genome, and gene-level read counting. Normalization and differential expression analysis were performed using the NEGEDIA degsanalysis pipeline (v1.2.0). Specifically, sequence reads were trimmed using BBDuk software to remove adapter sequences, poly-A tails, and low-quality end bases. Alignment was performed with STAR 2.6.0a on hg38 reference genome assembly. Gene expression levels were determined using HTseq-counts 0.9.1. Differentially expressed genes (DEGs) were identified using the following thresholds: $\log_2$(Fold Change) ≥ 1.5 or ≤ -1.5 and adjusted p-value (pAdj) ≤ 0.05. A total of 43 significantly downregulated and 116 significantly upregulated genes in MWS cells compared to controls are listed in Supplementary File.

Gene Ontology (GO) enrichment analysis was performed on these DEGs using the ShinyGO v.0.82 online tool (Ge et al., 2020) restricting the output to Biological Process, Cellular Component, Molecular Function, and KEGG categories. A false discovery rate (FDR) cutoff of <0.05 was applied for term selection. All transcripts detected in the experiment were used as the background set.

2.10. Accession codes

The RNA-seq data discussed in this publication have been deposited in NCBI's Gene Expression Omnibus and are accessible through GEO Series accession number GSE311389 (https://www.ncbi.nlm.nih.gov/geo/query/acc.cgi?acc=GSE311389).

2.11. Holographic imaging and analysis

Label-free live imaging of NPCs and neurons seeded on Geltrex-coated 24-well plates (82,426, IBIDI) was performed using the Holomonitor M4 imaging system, equipped with a motorized xyz-stage and 20× objective (Phase Holographic Imaging PHI AB). Live-cell holographic imaging was conducted according to the manufacturer's instructions. For NPCs, images were acquired every 10 min over a total duration of 16 h. During neuronal differentiation, images were captured every 30 min for a total of 65 h between medium changes.

Image processing and analysis were performed with APP Suite Cell Imaging Software (Phase Holographic Imaging PHI AB), employing the Kinetic Cell Motility, Kinetic Cell Proliferation, and Cell Quality Control assays. Cell segmentation and identification were automatically performed using an adaptive Gaussian threshold method with a threshold value set at 135 and a minimum cell size of 16, consistently applied across all wells and positions. The following dynamic and morphological features were quantified: cell count, confluence, mean cell volume, mean cell area, mean cell diameter, mean cell speed, accumulated cell distance.

2.12. Data presentation and statistical analysis

All graphs and figures were generated using Igor Pro 9 (WaveMetrics). Data are presented as representative images and quantitative graphs displaying individual data points along with the mean ± S.D., obtained from independent biological replicates. The exact number of biological replicates for each experiment is specified in the corresponding figure legends. Statistical analyses were performed by grouping data according to condition (C1 and C2 as controls; P1-P4 as patient-derived lines). The association of marker expression, genes, and other cell measures, such as mean cell speed, volume, area, etc., with case-control status was tested using linear mixed-effects regression models. The cell status (case-control) was included as a fixed effect, while cell ID was treated as a random effect to take into account the repeated measurements associated with the same cell line. Analyses were conducted using the *lmer* function within the *lme4* package (version 1.1–37) in R.

3. Results

3.1. Generation and validation of iPSC lines carrying ZEB2 variants

We successfully generated iPSCs from four MWS patients carrying distinct pathogenic variants in the *ZEB2* gene, each associated with well-documented clinical phenotypes (Table 1). The following variants (all referred to transcript NM_014795.4) were modelled: c.2682del (P1), c.650_653dup (P2), c.817del (P3), and c.1578_1579delinsA (P4). Variants in patients P1 and P4 are in exon 8, while those in P2 and P3 reside in exons 6 and 7, respectively (Fig. 1A). All variants introduce frameshifts predicted to trigger nonsense-mediated mRNA decay, consistent with *ZEB2* haploinsufficiency. PBMCs were reprogrammed using a standard Sendai virus-based protocol. Sanger sequencing confirmed the presence of the *ZEB2* variants in the iPSC clones, and RT-PCR analysis verified the loss of exogenous reprogramming factor expression (Fig. 1B,

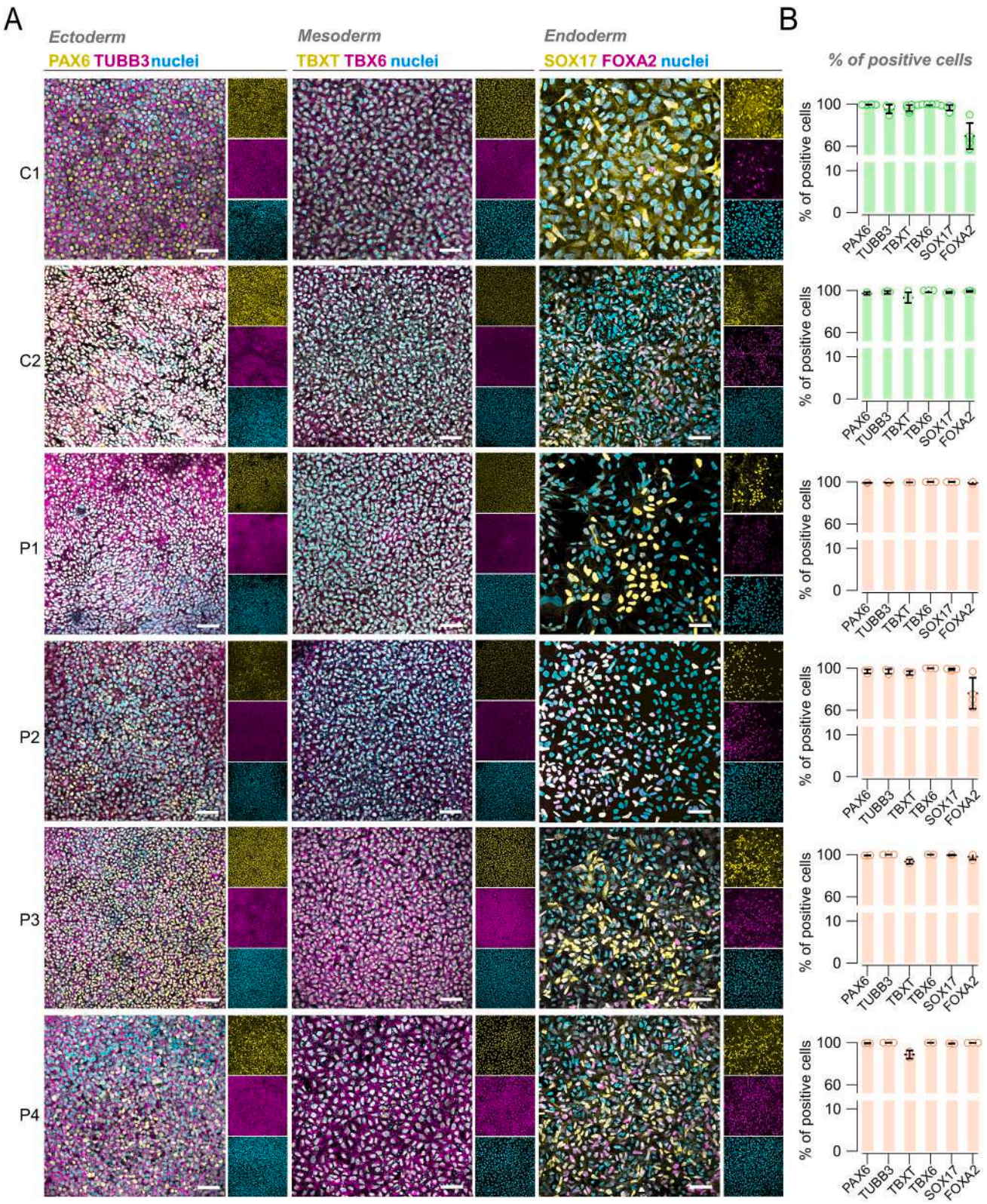

Fig. 2. Pluripotency analysis of MWS iPSCs lines. The ability of MWS iPSC lines to differentiate into all three germ layers was assessed via in vitro differentiation followed by immunofluorescence analysis of lineage-specific markers. (A) Representative confocal images showing expression of ectodermal (PAX6, β3-tubulin), mesodermal (TBXT, TBX6), and endodermal (SOX17, FOXA2) markers. (B) Quantification of marker expression across control and patient-derived iPSC lines. Scale bar: 25 μm. Bar graphs represent mean ± S.D.; individual biological replicates are shown as dots ($n = 3$–6). Statistical analysis was performed by grouping data by condition (C1 and C2 as controls vs. P1-P4 as patient-derived lines). No statistically significant differences were detected by linear mixed models.

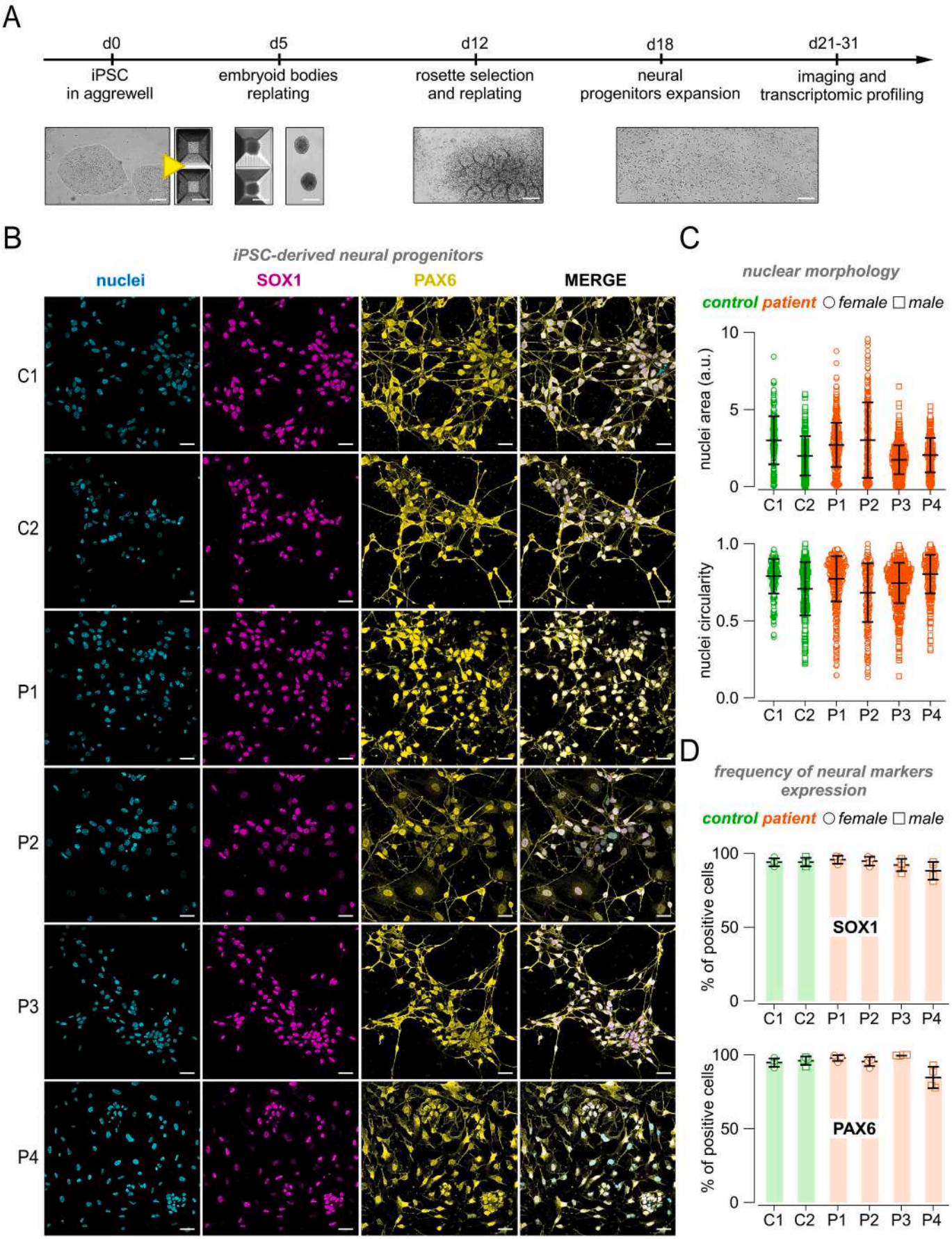

(caption on next page)

Fig. 3. Generation of iPSC-derived neural progenitors (NPC). (A) Schematic timeline of the multistep neural induction process, with representative brightfield images showing the progression from iPSCs to embryoid bodies, neural rosettes, and neural progenitor cells (NPCs). (B) Representative confocal images of iPSC-NPCs stained for SOX1 and PAX6, typical markers of early neural identity. Scale bar: 50 μm. (C) Dot plot graphs showing quantification of nuclear morphology (size and shape) in NPCs. At least 200 cells were analyzed for each line. (D) Quantitative analysis of the percentage of cells expressing neural markers, based on high-content imaging of samples as shown in panel B. Bar graphs represent mean ± S.D.; individual biological replicates are shown as dots ($n = 4$). Statistical analysis was performed by grouping data by condition (C1 and C2 as controls vs. P1-P4 as patient-derived lines). No statistically significant differences were detected by linear mixed models.

C). Immunofluorescence analysis demonstrated that patient-derived iPSC lines robustly expressed canonical undifferentiated state markers (OCT4, SSEA4, SOX2, and TRA-1-60), at levels comparable to those of previously established control lines, with more than 90 % of cells expressing each marker (Fig. 1D-E).

3.2. MWS iPSCs retain pluripotency and can differentiate into all three germ layers

We next evaluated the differentiation potential of MWS iPSC lines. Upon in vitro differentiation, both control and patient-derived lines were capable of generating cells expressing markers of the three germ layers: PAX6 and β3-tubulin for ectoderm, TBXT and TBX6 for mesoderm, and SOX17 and FOXA2 for endoderm (Fig. 2A). Quantitative analysis confirmed similarly high levels of lineage-specific marker expression across lines (Fig. 2B), supporting that MWS iPSCs retain full pluripotency.

3.3. Efficient generation of neural progenitor cells from MWS iPSCs

To model early neural development, iPSCs were differentiated into neural progenitor cells (NPCs) following a standard dual-SMAD inhibition protocol involving the sequential generation of embryoid bodies, neural rosettes, and NPCs (Fig. 3A). Immunostaining confirmed expression of early neural markers SOX1 and PAX6 in both control and MWS-derived NPCs (Fig. 3B). Morphometric analysis revealed no significant differences in nuclear shape or size (Fig. 3C), and the proportion of SOX1/PAX6-positive cells was comparable across lines (Fig. 3D), indicating efficient and consistent neural induction.

3.4. Transcriptional profiling reveals altered neural identity in MWS NPCs

RNA-seq analysis of iPSC-derived NPCs uncovered significant transcriptional alterations in MWS lines compared to controls. To explore potential changes in cell identity, we focused on panels of genes representing established markers of different brain cell lineages (Ianevski et al., 2022) (Fig. 4). Both control and MWS NPCs showed lack of expression of pluripotency genes, including *NANOG*, *TDGF1*, *FGF4*, and *DPPA2*, confirming exit from the undifferentiated state (Fig. 4A). Lineage-specific markers revealed more subtle differences. Early neuroepithelial genes such as *NOTCH1*, *HES1*, *SOX1*, and *SOX2* were expressed at comparable levels between groups, whereas radial glial markers *NES*, *PAX6*, and *SLC1A3* were significantly reduced in MWS NPCs (Fig. 4A, B). Within the glial lineage markers, MWS NPCs showed a trend toward reduced expression of the Schwann cell precursor marker *GAP43* and increased expression of the oligodendrocyte precursor cell (OPC) marker *CSPG4*, although these differences did not reach statistical significance (Fig. 4C, D). As expected at this developmental stage, markers of mature glial cells (including Schwann cells, oligodendrocytes, and astrocytes) remained largely silent across all samples, except for *NCAM1*, which showed relatively high expression (Fig. 4C). Early and mature neuronal markers were also examined. The neurogenic regulators *ASCL1* and *DCX* were expressed at high levels, with slight reductions observed in three out of the four patient lines (Fig. 4E, F). Markers of mature neurons, such as *SYP* and *SLC16A7*, were expressed at very low levels, while GABAergic neuronal markers including *SLC32A1*, *GAD1*, and *GAD2* showed medium-low expression in controls and variable, often reduced, expression in MWS lines (Fig. 4E, F). When comparing all control versus all MWS NPCs as groups, these differences did not reach statistical significance (Fig. 4E, F).

Altogether, these findings indicate that *ZEB2* variants alter transcriptional programs governing radial glial development and may subtly influence neuronal subtype specification, which could contribute to neurodevelopmental deficits in MWS.

3.5. Differential gene expression and pathway enrichment in MWS NPCs

To investigate global gene expression changes, we performed differential expression analysis between MWS and control iPSC-derived NPCs. We identified 43 significantly downregulated and 116 significantly upregulated genes in MWS cells compared to controls (Fig. 5A). The top 40 differentially expressed genes in each group are shown in Fig. 5B and C.

Notably, downregulated genes with known roles in neurogenesis included *CER1* (a cytokine essential for anterior neural induction), *PCP4* (a positive regulator of neuronal differentiation), *BEND6* (which promotes neuronal differentiation by repressing neural stem cell self-renewal), *SLCO1C1* (an organic anion transporter involved in GABAergic interneuron development), *SPARCL1* (involved in synapse formation), *CACNB2* (which encodes a beta subunit of voltage-gated calcium channels), and *DOC2B* (a calcium sensor critical for synaptic vesicle release) (Dai et al., 2013; Diez et al., 2021; Friedrich et al., 2008; Friedrich et al., 2008; Hou et al., 2013; Kucukdereli et al., 2011; Martins et al., 2022; Mayerl et al., 2022; Mouton-Liger et al., 2011). Additionally, some downregulated genes have been also implicated in neurodevelopmental disorders: *GABBR2* (developmental and epileptic encephalopathy), *CPNE6* (epilepsy and neuromuscular disease), *KCNN3* (Zimmermann-Laband syndrome-3), and *MCHR1* (linked to bipolar disorders) (Anazi et al., 2017; Bauer et al., 2019; Gripp et al., 2021; Mullins et al., 2021; Yoo et al., 2017).

Conversely, many upregulated genes in MWS NPCs were associated with extracellular matrix remodeling and non-neural lineage specification. Among the former, we found ECM structural genes (*COL1A1, COL1A2, COL5A1, COL12A1, COL13A1, COL26A1*), ECM-associated glycoproteins (*FBLN2, EMILIN1, EGFL6, NID2, HAPLN1*), ECM modulators (*MMP25, PCOLCE*), adhesion-related genes (*CD248, KIRREL2, ITGA5*, *ISLR, DSP, CLDN11*), and migration and matrix signaling genes (*EMCN*, *LAMC3*) (Theocharis et al., 2016). Regarding non-neural lineage specification, we found up-regulation of genes involved in vascular development, including *EMILIN1* and *PEAR1* (vascular stability and adhesion), *CASZ1*, *EDNRA*, *ADGRA2*, and *PLXDC1* (angiogenesis and vessel remodeling), *APLNR*, *ANGPT2*, and *ENG* (angiogenesis signaling) (Adamo et al., 2022; Akwii et al., 2019; Eubelen et al., 2018; Liu et al., 2023; Mughal and O'Rourke, 2018; Vandenbriele et al., 2015). Furthermore, upregulation of genes involved in skeletal development (e.g., *OGN*, *BGN*, *CREB3L1*, *ITM2A*, *KAZALD*, *MSX2*) and Wnt signaling regulators (e.g., *DKK2*, *FRZB*) was also observed, suggesting aberrant activation of non-neural developmental programs in MWS NPCs (Berendsen et al., 2014; Bodine and Komm, 2006; Hock et al., 2001; Keller et al., 2018; Lories et al., 2013).

Gene Ontology (GO) enrichment analyses based on DEGs revealed a substantially higher number of enriched pathways among upregulated genes. KEGG pathway analysis highlighted significant enrichment in pathways associated with protein digestion and absorption, PI3K-Akt signaling, Relaxin signaling, focal adhesion, and extracellular matrix

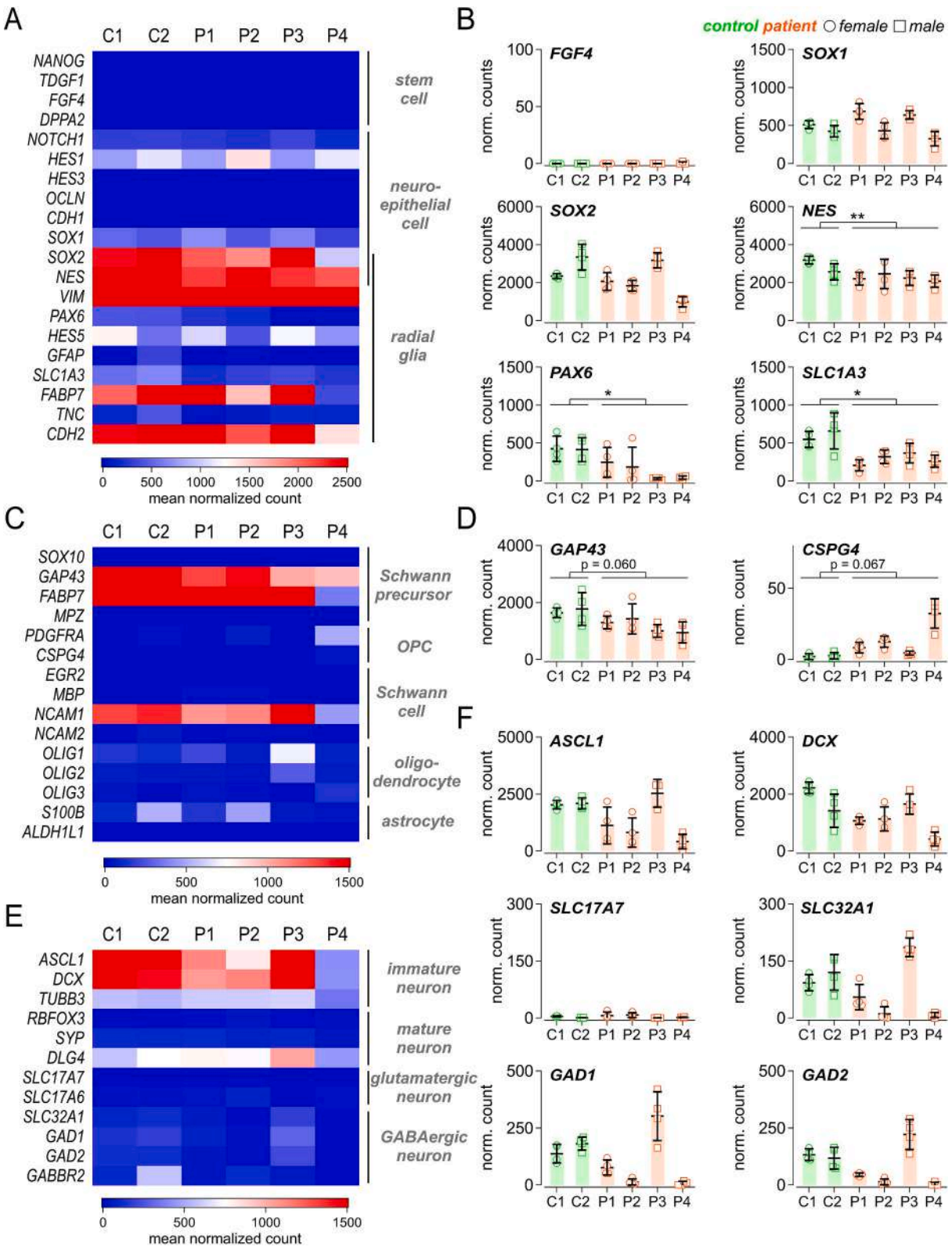

Fig. 4. Transcriptional profiling of MWS iPSC-derived NPCs. (A, C, E) Heatmaps showing mean normalized expression levels of genes associated with distinct neural cell identities and developmental states. (A) Markers of stem cells, neuroepithelial cells, and radial glia. (C) Markers of Schwann cell precursors, oligodendrocyte precursor cells (OPCs), Schwann cells, oligodendrocytes, and astrocytes. (E) Markers of immature neurons, mature neurons, glutamatergic neurons, and GABAergic neurons. (B, D, F) Quantitative plots of normalized expression levels for selected genes shown in the corresponding heatmaps. Bar graphs represent mean ± S.D.; individual biological replicates are shown as dots (n = 4). Statistical analysis was performed by grouping data by condition (C1 and C2 as controls vs. P1-P4 as patient-derived lines). *, $p < 0.05$; **, $p < 0.01$ determined by linear mixed models.

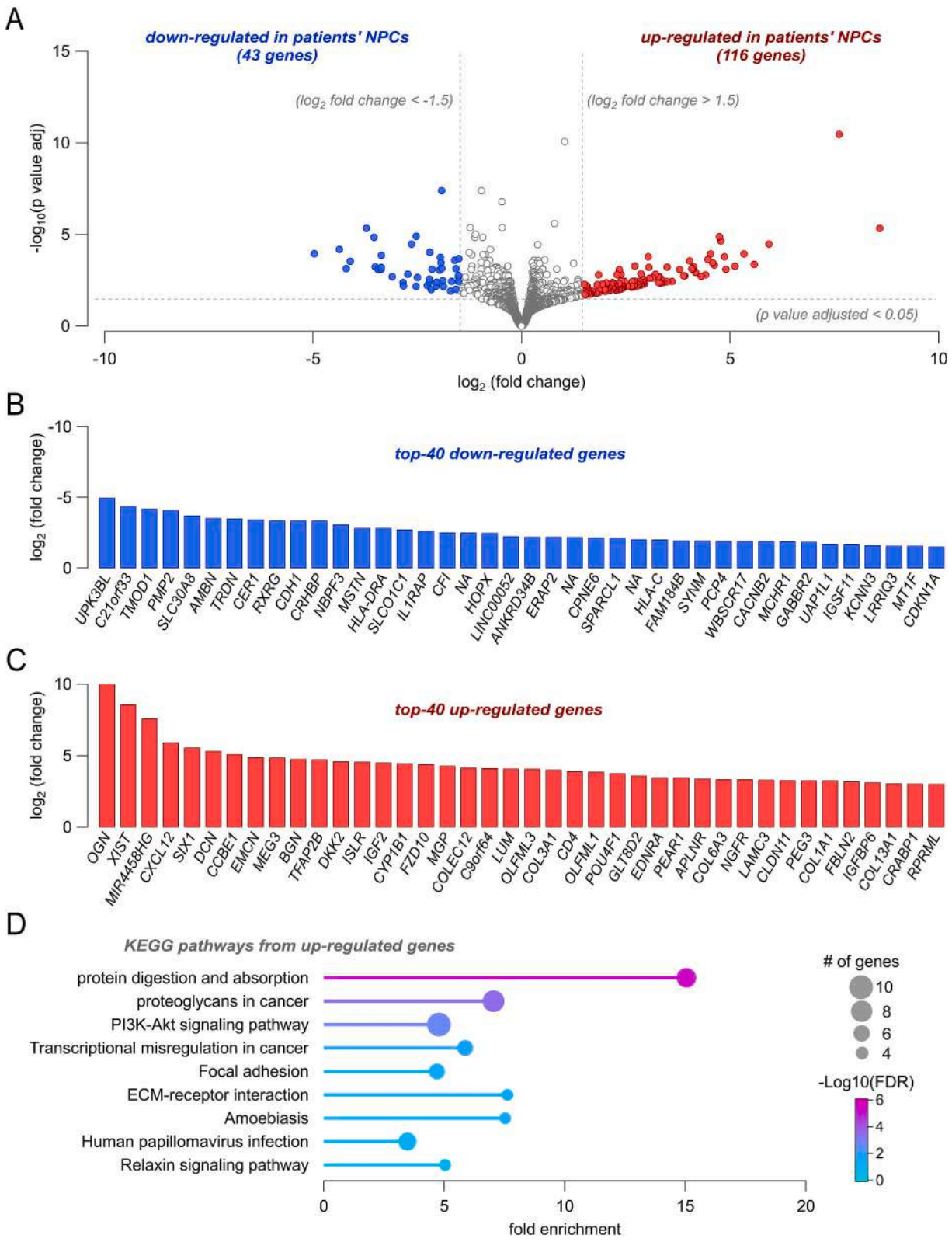

Fig. 5. Analysis of differentially expressed genes in MWS iPSC-derived NPCs. (A) Volcano plot showing differentially expressed genes (DEGs) between control and patient iPSC-derived NPCs from RNA-seq data. Genes with $\log_2$ fold change < -1.5 and adjusted $p < 0.05$ are shown in blue; those with $\log_2$ fold change >1.5 and adjusted $p < 0.05$ are shown in red; non-significant genes ($-1.5 < \log_2$ fold change <1.5 and/or adjusted $p > 0.05$) are shown in gray. (B, C) Bar plots of the top 40 significantly downregulated (B) and upregulated (C) genes in MWS NPCs compared to controls. (D) Gene Ontology enrichment analysis of up-regulated genes, highlighting KEGG pathways ranked by fold enrichment, false discovery rate (FDR), and number of differentially expressed genes per pathway. All analyses were performed using transcriptomic data from four preparations of iPSC-derived NPCs (n = 4). (For interpretation of the references to colour in this figure legend, the reader is referred to the web version of this article.)

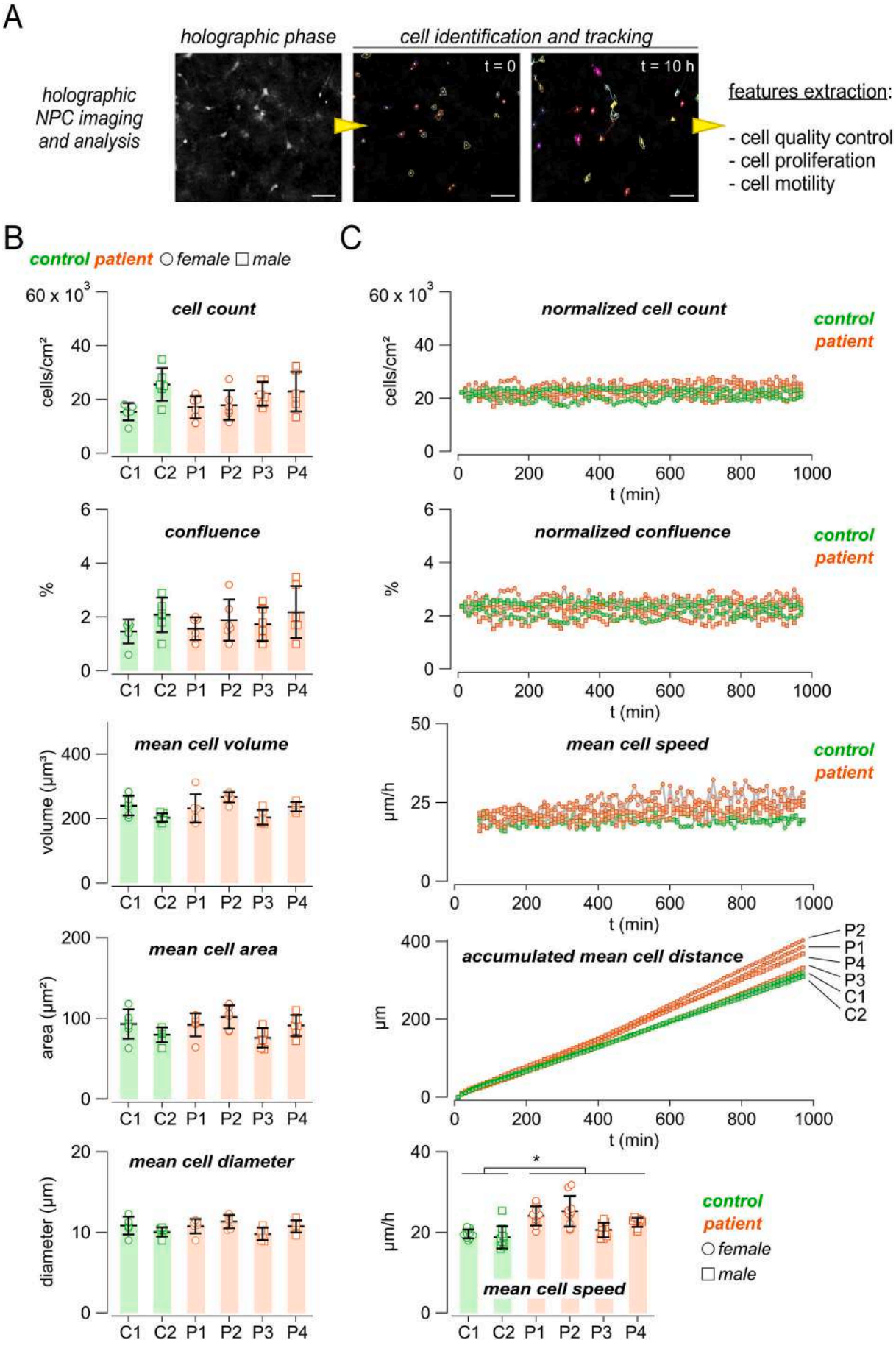

(caption on next page)

Fig. 6. Label-free imaging of MWS iPSC-derived NPCs. Holographic live-imaging of iPSC-derived NPC revealed comparable basic morphology but increased motility in MWS-derived cells. Control and patient iPSC-derived NPCs were seeded in 24-well plates and imaged every 10 min at 20× magnification over a 16-h period using label-free holographic microscopy. (A) Representative holographic phase image before (left) and after (right) cell segmentation and tracking. Scale bar: 50 μm. (B) Summary graphs showing output variables measured after 1 h: cell count, confluence, mean cell volume, mean cell area, and mean cell diameter. Bar graphs represent mean ± S.D.; individual biological replicates are shown as dots ($n = 6$). No statistically significant differences were detected by linear mixed models. (C) Summary graphs showing dynamic output variables over the 16-h imaging period: normalized cell count and confluence (values normalized to the mean of all conditions at time 0), mean cell speed, and accumulated mean cell distance. The bottom graph shows mean cell speed averaged per cell line. Bar graphs represent mean ± S.D.; individual biological replicates are shown as dots (n = 6). Statistical analysis was performed by grouping data by condition (C1 and C2 as controls vs. P1-P4 as patient-derived lines). *, $p < 0.05$ as determined by linear mixed models ($n = 10$ replicates from 3 independent cell preparations).

(ECM) interaction in upregulated genes, while no significant enrichment was found among downregulated genes (Fig. 5D). Consistently, GO analysis showed that upregulated genes were enriched in biological processes such as vasculature development, tube morphogenesis, and system development, in cellular components like collagen-containing extracellular matrix, and in molecular functions including ECM structural constituents and DNA-binding transcription factor activity (Supplementary Fig. 1). In contrast, downregulated genes were modestly enriched in GO categories related to antigen processing, cellular response to metal ions, and endoplasmic reticulum components (Supplementary Fig. 2).

Together, these results reveal critical transcriptional dysregulation in MWS NPCs, characterized by impaired neurogenic programs and aberrant activation of extracellular matrix and non-neural developmental pathways, potentially contributing to the neuropathological and systemic features of Mowat-Wilson syndrome.

3.6. Increased cell motility in MWS NPCs and early neurons

To explore the functional consequences of transcriptional dysregulation, we performed label-free holographic live imaging of NPCs. While overall growth and morphological metrics, including cell count, confluence, mean cell volume, area, and diameter, were comparable between groups, MWS NPCs exhibited significantly increased motility, as evidenced by higher cell speed and greater accumulated distance over time (Fig. 6A-C). These findings are consistent with transcriptomic data indicating dysregulation of ECM interaction pathways and suggest that *ZEB2* dysfunction affects the dynamic behavior of neural progenitor cells.

To assess whether these alterations persisted during early neuronal differentiation, MWS and control NPCs were further differentiated into early neurons and monitored by holographic imaging over a 10-day period. Increased motility was observed in MWS-derived cells during the initial stages of differentiation (day 1), but this difference disappeared at later time points (Fig. 7A-B). Despite these early dynamic differences, immunofluorescence analysis at day 10 revealed no significant differences in the proportion of MAP2-positive neurons, nor in MAP2 signal intensity or positive area (Fig. 7C–D), indicating that early neuronal maturation is maintained in MWS cells despite altered motility behavior.

4. Discussion

This study expands our understanding of *ZEB2*-associated neurodevelopmental dysfunction by employing patient-derived iPSC models of MWS. Through transcriptomic and phenotypic analyses of neural progenitor cells (NPCs) and early neurons, we demonstrate that *ZEB2* haploinsufficiency disrupts key processes in early neural development, including radial glial maturation, neuronal specification, ECM regulation, and cell motility.

Consistent with the known role of *ZEB2* in neurodevelopment (Epifanova et al., 2019; Tomassy et al., 2013; van den Berghe et al., 2013), MWS-derived NPCs exhibited transcriptional alterations affecting both neurogenic and glial lineage programs. The significant downregulation of radial glial markers such as *NES*, *PAX6*, and *SLC1A3* suggests a defective neuroepithelial-to-radial glia transition, in line with findings from animal models (Benito-Kwiecinski et al., 2021; Epifanova et al., 2019). Moreover, other downregulated genes are critical for neurogenesis and synaptic function (e.g., *CER1*, *PCP4*, *BEND6*, *SLCO1C1*, *SPARCL1*, *CACNB2*, *DOC2B*) and some have been implicated in neurodevelopmental disorders, including *GABBR2*, *CPNE6*, *KCNN3*, and *MCHR1* (Anazi et al., 2017; Bauer et al., 2019; Dai et al., 2013; Diez et al., 2021; Friedrich et al., 2008; Friedrich et al., 2008; Gripp et al., 2021; Hou et al., 2013; Kucukdereli et al., 2011; Martins et al., 2022; Mayerl et al., 2022; Mouton-Liger et al., 2011; Mullins et al., 2021; Yoo et al., 2017). These observations support the notion that *ZEB2* dysfunction perturbs early neural lineage specification and maturation, potentially contributing to the excitation-inhibition imbalance and neurodevelopmental deficits underlying epilepsy in MWS.

Importantly, we identified substantial transcriptional upregulation of genes associated with ECM organization and non-neural lineages, including vasculature and skeletal development. Elevated expression of *COL1A1*, *MMP25*, *FBLN2*, *ANGPT2*, and *DKK2*, among others, points to aberrant activation of mesodermal and endothelial programs in neural cultures. This suggests a failure of *ZEB2*-deficient NPCs to properly repress alternative lineage trajectories, consistent with *ZEB2*'s known role in lineage restriction and epithelial-mesenchymal transition (EMT) pathways (Vandewalle et al., 2005; Ninfali et al., 2023; Charney et al., 2023; Chng et al., 2010). The upregulation of vasculature-related genes may also provide a molecular link to systemic MWS manifestations such as cardiovascular anomalies and connective tissue involvement (Epifanova et al., 2019; St Peter et al., 2024).

A particularly intriguing finding of our study is the increased motility of MWS-derived NPCs and early neurons, as revealed by label-free holographic live imaging. While previous studies in animal models have reported defective migration of *ZEB2*-deficient interneurons, our data show that MWS cells exhibit increased intrinsic motility, moving more rapidly and covering greater distances in vitro. However, motility and migration are distinct phenomena: motility refers to a cell's inherent ability to move, while migration implies directed, context-specific movement often guided by environmental cues. Our findings suggest that, although MWS cells are more motile, they may lack the necessary directional control for proper migration in vivo. This may stem from dysregulation of ECM genes, adhesion molecules, or cytoskeletal regulators that coordinate migration and positioning. Thus, *ZEB2* dysfunction may decouple intrinsic motility and functional migration in MWS, underscoring the need for future studies using spatially structured systems (e.g., microfluidic devices or 3D models) to assess directed migration during human brain development.

Interestingly, while global downregulation of neurogenic pathways was evident, the number of significantly downregulated genes was relatively small compared to the larger set of upregulated genes. This imbalance between upregulated and downregulated transcripts may reflect the dominant repressive role of *ZEB2* on non-neural genes and the secondary consequences of losing this repression during neural differentiation (Ninfali et al., 2023). Alternatively, it could indicate a compensatory response attempting to maintain neural identity in the absence of proper transcriptional cues.

In this study, molecular and functional profiling were performed by comparing all control NPC lines as a group versus all MWS lines as a group. Although our group-level analysis successfully revealed shared disease-associated signatures across multiple patient lines, it may also

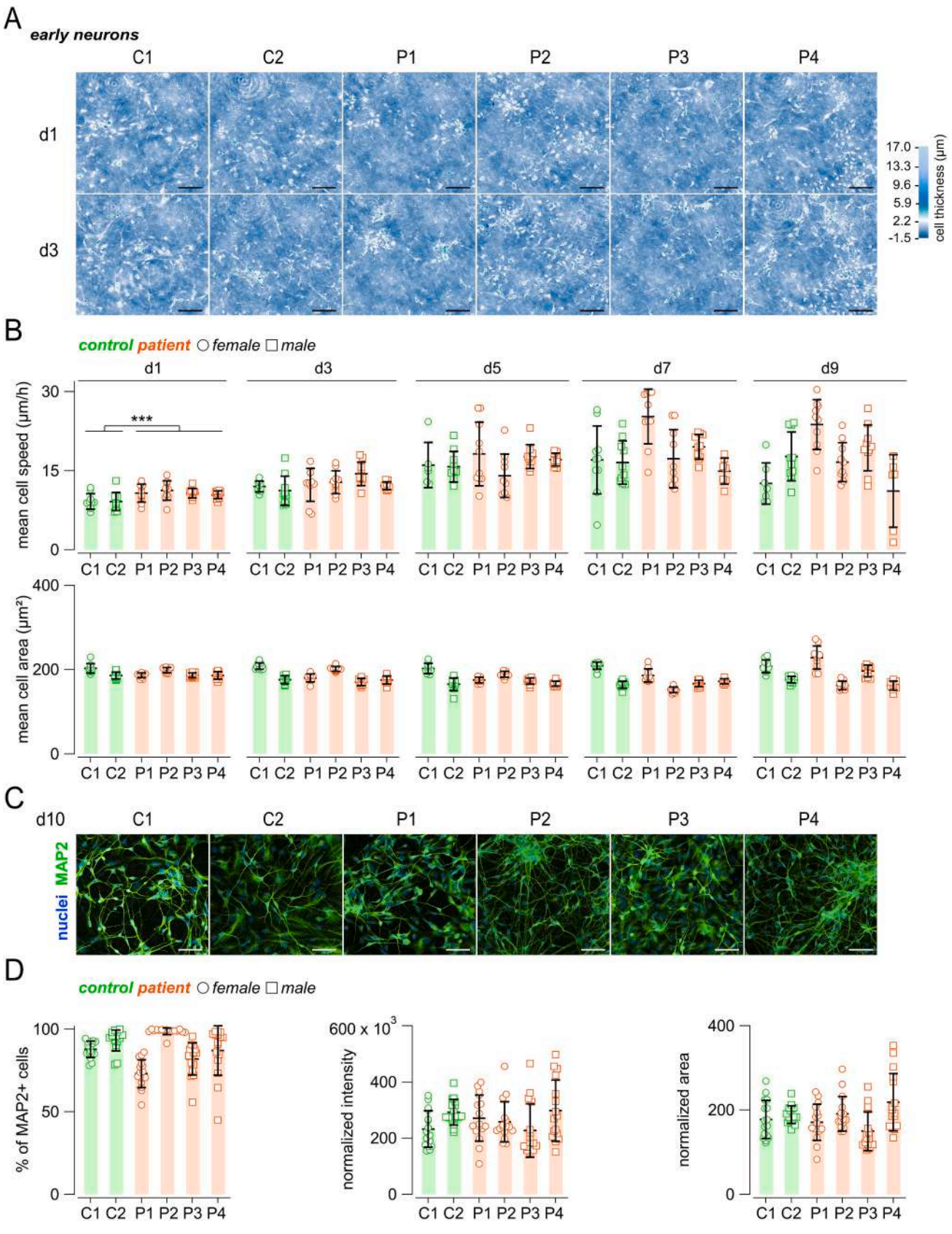

(caption on next page)

Fig. 7. Altered motility in MWS early neurons. Control and MWS iPSC-derived NPCs were induced to differentiated into early neurons and monitored via holographic live-cell imaging for 10 days. On day 10, cells were fixed and stained for the neuronal marker MAP2. (A) Representative holographic phase images of early neurons at day 1 (d1) and day 3 (d3) for control and MWS-derived lines. Colour scale indicates cell thickness. Scale bar: 100 μm (B) Summary graphs showing mean cell speed (top) and mean cell area (bottom) at the indicated time points (d1, d3, d5, d7, and d9). Bar graphs represent mean ± S.D.; individual replicates are shown as dots (n = 10 replicates from 3 independent cell preparations). Statistical analysis was performed by grouping data by condition (C1 and C2 as controls vs. P1-P4 as patient-derived lines). ***, $p < 0.001$ as determined by linear mixed models. (C) Representative immunofluorescence images of early neurons at day 10 stained for MAP2 (green) and nuclei (blue). Scale bar: 100 μm. (D) Quantification of MAP2 expression in terms of frequency of expression (percentage of MAP2-positive cells), normalized intensity (total MAP2 signal intensity divided by the number of positive cells), and normalized area (total MPA2-positive area divided the number of positive cells). No statistically significant differences were detected (linear mixed models; $n = 16$ replicates from 4 independent cell preparations). (For interpretation of the references to colour in this figure legend, the reader is referred to the web version of this article.)

have masked variant- or line-specific effects. For example, the GABAergic neuronal markers *SLC32A1*, *GAD1*, and *GAD2* showed reductions in three out of four MWS lines. These findings are consistent with observations from animal models and previous iPSC-based studies (Benito-Kwiecinski et al., 2021; Epifanova et al., 2019; Schuster et al., 2022), indicating that *ZEB2* dysfunction perturbs interneurons maturation. Yet, these differences did not reach statistical significance in the aggregated dataset (Fig. 4F).

A systematic per-line comparison could therefore uncover distinct transcriptional signatures associated with specific *ZEB2* mutations and reveal potential genotype–phenotype correlations. However, rigorous assessment of such effects will require larger cohorts of independent iPSC lines per genotype and/or the generation of isogenic corrected controls to disentangle true variant-driven changes from line-to-line biological or technical variability. Addressing these aspects in future work will provide a more comprehensive understanding of *ZEB2*'s diverse regulatory roles and refine our interpretation of patient-specific molecular phenotypes in MWS.

Collectively, our results indicate that *ZEB2* haploinsufficiency disrupts early human neurodevelopment through multiple, converging mechanisms: impaired lineage specification, dysregulation of neurogenic and non-neural transcriptional programs, and altered progenitor cell dynamics. These disruptions likely contribute to core clinical features of MWS, including intellectual disability, epilepsy, and brain structural anomalies such as corpus callosum hypoplasia. Future studies should extend these findings by examining later stages of neuronal maturation, synaptic function, and interneuron network activity using long-term differentiated cultures and electrophysiological analyses.

5. Conclusion

This study advances our understanding of *ZEB2*'s role in human neurodevelopment and provides a robust platform for further exploration of MWS pathogenesis. By generating and thoroughly validating high-quality iPSC lines from four unrelated MWS patients carrying distinct *ZEB2* variants, each with well-documented clinical profiles, we have established a valuable and reproducible human-based model system. These patient-specific iPSCs not only recapitulate key molecular and cellular features of the disorder but also represent a critical resource for future mechanistic investigations. Their application will enable deeper exploration of *ZEB2*-regulated transcriptional and epigenetic programs, interneuron specification, and cortical circuit formation, particularly in relation to seizure pathophysiology. Importantly, these patient-derived in vitro models also pave the way for precision medicine approaches, including genotype–phenotype correlation studies, high-throughput drug screening, and the development of targeted therapeutic strategies aimed at restoring *ZEB2* function or correcting downstream dysregulated pathways in MWS.

CRediT authorship contribution statement

Ilaria Musante: Visualization, Validation, Methodology, Investigation, Formal analysis. **Giulia Gorrieri:** Visualization, Methodology, Investigation. **Serena Tamburro:** Methodology, Investigation. **Giulia Ferrera:** Resources. **Simona Baldassari:** Methodology, Investigation. **Anna Fetta:** Resources. **Stefano Giuseppe Caraffi:** Resources, Formal analysis. **Aglaia Vignoli:** Resources. **Giovanni Fiorito:** Writing – review & editing, Data curation. **Livia Garavelli:** Resources. **Maria Paola Canevini:** Supervision, Resources. **Duccio Maria Cordelli:** Supervision, Resources. **Federico Zara:** Supervision, Resources. **Emilia Ricci:** Writing – review & editing, Project administration, Funding acquisition, Conceptualization. **Paolo Scudieri:** Writing – review & editing, Writing – original draft, Visualization, Supervision, Resources, Project administration, Funding acquisition, Formal analysis, Conceptualization.

Consent to participate

Informed consent was obtained from all individual participants included in the study.

Consent to publish.

na

Ethics approval

This study was performed in line with the principles of the Declaration of Helsinki. Approval was granted by the Ethics Committee of University of Milan (protocol number 11/23, dated 18 January 2023).

Funding

This study was supported by a grant from Fondazione LICE and Associazione Italiana Mowat-Wilson to ER and PS. This study was also supported by the Italian Ministry of Health through 5 × 1000 (5M-2022-23685494 to PS and 5M-2017-23684149 to FZ).

Declaration of competing interest

The authors declare that they have no known competing financial interests or personal relationships that could have appeared to influence the work reported in this paper.

Acknowledgements

The authors are deeply grateful to the "Fondazione Epilessia LICE" (Italian League Against Epilepsy Foundation) for its support and for believing in this project, which was made possible in collaboration with the Italian Mowat-Wilson Association. The authors also acknowledge the Biobank of the Laboratory of Human Genetics at IRCCS Istituto Giannina Gaslini, member of the Telethon Network of Genetic Biobanks (GTB18001), funded by Telethon Italy, and by EuroBioBank Network which provided us with PBMCs and DNA collected from MWS patients. The authors are members of the European Reference Network on Rare Congenital Malformations and Rare Intellectual Disability (ERN-ITHACA) and the European Reference Network on Rare and Complex Epilepsies (ERN EpiCARE). ERN-ITHACA is funded by the European Union under Grant Agreement No. 101156387. ERN EpiCARE is funded by the European Union under Grant Agreement No. 769051.

Appendix A. Supplementary data

Supplementary data to this article can be found online at https://doi.org/10.1016/j.nbd.2025.107205.

Data availability

All relevant data are included in the manuscript and its supporting information files. The RNA-seq data discussed in this publication have been deposited in NCBI's Gene Expression Omnibus and are accessible through GEO Series accession number GSE311389. Additional information may be obtained from the corresponding author upon request.

References

Adamo, C.S., Beyens, A., Schiavinato, A., Keene, D.R., Tufa, S.F., Mörgelin, M., Brinckmann, J., Sasaki, T., Niehoff, A., Dreiner, M., Pottie, L., Muiño-Mosquera, L., Gulec, E.Y., Gezdirici, A., Braghetta, P., Bonaldo, P., Wagener, R., Paulsson, M., Bornaun, H., De Rycke, R., De Bruyne, M., Baeke, F., Devine, W.P., Gangaram, B., Tam, A., Balasubramanian, M., Ellard, S., Moore, S., Symoens, S., Shen, J., Cole, S., Schwarze, U., Holmes, K.W., Hayflick, S.J., Wiszniewski, W., Nampoothiri, S., Davis, E.C., Sakai, L.Y., Sengle, G., Callewaert, B., 2022. EMILIN1 deficiency causes arterial tortuosity with osteopenia and connects impaired elastogenesis with defective collagen fibrillogenesis. Am. J. Hum. Genet. 109, 2230–2252. https://doi.org/10.1016/j.ajhg.2022.10.010.

Akwii, R.G., Sajib, M.S., Zahra, F.T., Mikelis, C.M., 2019. Role of Angiopoietin-2 in vascular physiology and pathophysiology. Cells 8, 471. https://doi.org/10.3390/cells8050471.

Anazi, S., Maddirevula, S., Faqeih, E., Alsedairy, H., Alzahrani, F., Shamseldin, H.E., Patel, N., Hashem, M., Ibrahim, N., Abdulwahab, F., Ewida, N., Alsaif, H.S., Al Sharif, H., Alamoudi, W., Kentab, A., Bashiri, F.A., Alnaser, M., AlWadei, A.H., Alfadhel, M., Eyaid, W., Hashem, A., Al Asmari, A., Saleh, M.M., AlSaman, A., Alhasan, K.A., Alsughayir, M., Al Shammari, M., Mahmoud, A., Al-Hassnan, Z.N., Al-Husain, M., Osama Khalil, R., Abd El Meguid, N., Masri, A., Ali, R., Ben-Omran, T., El Fishway, P., Hashish, A., Ercan Sencicek, A., State, M., Alazami, A.M., Salih, M.A., Altassan, N., Arold, S.T., Abouelhoda, M., Wakil, S.M., Monies, D., Shaheen, R., Alkuraya, F.S., 2017. Clinical genomics expands the morbid genome of intellectual disability and offers a high diagnostic yield. Mol. Psychiatry 22, 615–624. https://doi.org/10.1038/mp.2016.113.

Aprile, D., Fruscione, F., Baldassari, S., Fadda, M., Ferrante, D., Falace, A., Buhler, E., Sartorelli, J., Represa, A., Baldelli, P., Benfenati, F., Zara, F., Fassio, A., 2019. TBC1D24 regulates axonal outgrowth and membrane trafficking at the growth cone in rodent and human neurons. Cell Death Differ. 26, 2464–2478. https://doi.org/10.1038/s41418-019-0313-x.

Bauer, C.K., Schneeberger, P.E., Kortüm, F., Altmüller, J., Santos-Simarro, F., Baker, L., Keller-Ramey, J., White, S.M., Campeau, P.M., Gripp, K.W., Kutsche, K., 2019. Gain-of-function mutations in KCNN3 encoding the small-conductance Ca2+-activated K + channel SK3 cause Zimmermann-Laband syndrome. Am. J. Hum. Genet. 104, 1139–1157. https://doi.org/10.1016/j.ajhg.2019.04.012.

Benito-Kwiecinski, S., Giandomenico, S.L., Sutcliffe, M., Riis, E.S., Freire-Pritchett, P., Kelava, I., Wunderlich, S., Martin, U., Wray, G.A., McDole, K., Lancaster, M.A., 2021. An early cell shape transition drives evolutionary expansion of the human forebrain. Cell 184, 2084–2102 e19. https://doi.org/10.1016/j.cell.2021.02.050.

Berendsen, A.D., Pinnow, E.L., Maeda, A., Brown, A.C., McCartney-Francis, N., Kram, V., Owens, R.T., Robey, P.G., Holmbeck, K., de Castro, L.F., Kilts, T.M., Young, M.F., 2014. Biglycan modulates angiogenesis and bone formation during fracture healing. Matrix Biol. 35, 223–231. https://doi.org/10.1016/j.matbio.2013.12.004.

Bodine, P.V.N., Komm, B.S., 2006. Wnt signaling and osteoblastogenesis. Rev. Endocr. Metab. Disord. 7, 33–39. https://doi.org/10.1007/s11154-006-9002-4.

Caraffi, S.G., van der Laan, L., Rooney, K., Trajkova, S., Zuntini, R., Relator, R., Haghshenas, S., Levy, M.A., Baldo, C., Mandrile, G., Lauzon, C., Cordelli, D.M., Ivanovski, I., Fetta, A., Sukarova, E., Brusco, A., Pavinato, L., Pullano, V., Zollino, M., McConkey, H., Tartaglia, M., Ferrero, G.B., Sadikovic, B., Garavelli, L., 2024. Identification of the DNA methylation signature of Mowat-Wilson syndrome. Eur. J. Hum. Genet. 32, 619–629. https://doi.org/10.1038/s41431-024-01548-4.

Charney, R.M., Prasad, M.S., Juan-Sing, C., Patel, L.J., Hernandez, J.C., Wu, J., García-Castro, M.I., 2023. Mowat-Wilson syndrome factor ZEB2 controls early formation of human neural crest through BMP signaling modulation. Stem Cell Rep. 18, 2254–2267. https://doi.org/10.1016/j.stemcr.2023.10.002.

Chng, Z., Teo, A., Pedersen, R.A., Vallier, L., 2010. SIP1 mediates cell-fate decisions between neuroectoderm and mesendoderm in human pluripotent stem cells. Cell Stem Cell 6, 59–70. https://doi.org/10.1016/j.stem.2009.11.015.

Cordelli, D.M., Garavelli, L., Savasta, S., Guerra, A., Pellicciari, A., Giordano, L., Bonetti, S., Cecconi, I., Wischmeijer, A., Seri, M., Rosato, S., Gelmini, C., Della Giustina, E., Ferrari, A.R., Zanotta, N., Epifanio, R., Grioni, D., Malbora, B., Mammi, I., Mari, F., Buoni, S., Mostardini, R., Grosso, S., Pantaleoni, C., Doz, M., Poch-Olivé, M.L., Rivieri, F., Sorge, G., Simonte, G., Licata, F., Tarani, L., Terazzi, E., Mazzanti, L., Cerruti Mainardi, P., Boni, A., Faravelli, F., Grasso, M., Bianchi, P., Zollino, M., Franzoni, E., 2013. Epilepsy in Mowat-Wilson syndrome: delineation of the electroclinical phenotype. Am. J. Med. Genet. A 161A, 273–284. https://doi.org/10.1002/ajmg.a.35717.

Cordelli, D.M., Di Pisa, V., Fetta, A., Garavelli, L., Maltoni, L., Soliani, L., Ricci, E., 2021. Neurological phenotype of Mowat-Wilson syndrome. Genes (Basel) 12, 982. https://doi.org/10.3390/genes12070982.

Dai, Q., Andreu-Agullo, C., Insolera, R., Wong, L.C., Shi, S.-H., Lai, E.C., 2013. BEND6 is a nuclear antagonist of notch signaling during self-renewal of neural stem cells. Development 140, 1892–1902. https://doi.org/10.1242/dev.087502.

Di Pisa, V., Provini, F., Ubertiello, S., Bonetti, S., Ricci, E., Ivanovski, I., Caraffi, S.G., Giordano, L., Accorsi, P., Savasta, S., Raviglione, F., Boni, A., Grioni, D., Graziano, C., Garavelli, L., Cordelli, D.M., 2019. Sleep in Mowat-Wilson syndrome: a clinical and video-polysomnographic study. Sleep Med. 61, 44–51. https://doi.org/10.1016/j.sleep.2019.04.011.

Diez, D., Morte, B., Bernal, J., 2021. Single-cell transcriptome profiling of thyroid hormone effectors in the human Fetal neocortex: expression of SLCO1C1, DIO2, and THRB in specific cell types. Thyroid 31, 1577–1588. https://doi.org/10.1089/thy.2021.0057.

Engenheiro, E., Møller, R.S., Pinto, M., Soares, G., Nikanorova, M., Carreira, I.M., Ullmann, R., Tommerup, N., Tümer, Z., 2008. Mowat-Wilson syndrome: an underdiagnosed syndrome? Clin. Genet. 73, 579–584. https://doi.org/10.1111/j.1399-0004.2008.00997.x.

Epifanova, E., Babaev, A., Newman, A.G., Tarabykin, V., 2019. Role of Zeb2/Sip1 in neuronal development. Brain Res. 1705, 24–31. https://doi.org/10.1016/j.brainres.2018.09.034.

Epifanova, E., Salina, V., Lajkó, D., Textoris-Taube, K., Naumann, T., Bormuth, O., Bormuth, I., Horan, S., Schaub, T., Borisova, E., Ambrozkiewicz, M.C., Tarabykin, V., Rosário, M., 2021. Adhesion dynamics in the neocortex determine the start of migration and the post-migratory orientation of neurons. Sci. Adv. 7, eabf1973. https://doi.org/10.1126/sciadv.abf1973.

Eubelen, M., Bostaille, N., Cabochette, P., Gauquier, A., Tebabi, P., Dumitru, A.C., Koehler, M., Gut, P., Alsteens, D., Stainier, D.Y.R., Garcia-Pino, A., Vanhollebeke, B., 2018. A molecular mechanism for Wnt ligand-specific signaling. Science 361, eaat1178. https://doi.org/10.1126/science.aat1178.

Friedrich, R., Groffen, A.J., Connell, E., van Weering, J.R.T., Gutman, O., Henis, Y.I., Davletov, B., Ashery, U., 2008. DOC2B acts as a calcium switch and enhances vesicle fusion. J. Neurosci. 28, 6794–6806. https://doi.org/10.1523/JNEUROSCI.0538-08.2008.

Galanopoulou, A.S., 2010. Mutations affecting GABAergic signaling in seizures and epilepsy. Pflugers Arch. 460, 505–523. https://doi.org/10.1007/s00424-010-0816-2.

Galliera Genetic Bank: A DNA and Cell Line Biobank from Patients Affected by Genetic Diseases, 2016. Open J. Bioresour. 3, e1. https://doi.org/10.5334/ojb.15.

Garavelli, L., Ivanovski, I., Caraffi, S.G., Santodirocco, D., Pollazzon, M., Cordelli, D.M., Abdalla, E., Accorsi, P., Adam, M.P., Baldo, C., Bayat, A., Belligni, E., Bonvicini, F., Breckpot, J., Callewaert, B., Cocchi, G., Cuturilo, G., Devriendt, K., Dinulos, M.B., Djuric, O., Epifanio, R., Faravelli, F., Formisano, D., Giordano, L., Grasso, M., Grønborg, S., Iodice, A., Iughetti, L., Lacombe, D., Maggi, M., Malbora, B., Mammi, I., Moutton, S., Møller, R., Muschke, P., Napoli, M., Pantaleoni, C., Pascarella, R., Pellicciari, A., Poch-Olive, M.L., Raviglione, F., Rivieri, F., Russo, C., Savasta, S., Scarano, G., Selicorni, A., Silengo, M., Sorge, G., Tarani, L., Tone, L.G., Toutain, A., Trimouille, A., Valera, E.T., Vergano, S.S., Zanotta, N., Zollino, M., Dobyns, W.B., Paciorkowski, A.R., 2017. Neuroimaging findings in Mowat-Wilson syndrome: a study of 54 patients. Genet. Med. 19, 691–700. https://doi.org/10.1038/gim.2016.176.

Ge, S.X., Jung, D., Yao, R., 2020. ShinyGO: a graphical gene-set enrichment tool for animals and plants. Bioinformatics 36, 2628–2629. https://doi.org/10.1093/bioinformatics/btz931.

Gripp, K.W., Smithson, S.F., Scurr, I.J., Baptista, J., Majumdar, A., Pierre, G., Williams, M., Henderson, L.B., Wentzensen, I.M., McLaughlin, H., Leeuwen, L., Simon, M.E.H., van Binsbergen, E., Dinulos, M.B.P., Kaplan, J.D., McRae, A., Superti-Furga, A., Good, J.-M., Kutsche, K., 2021. Syndromic disorders caused by gain-of-function variants in KCNH1, KCNK4, and KCNN3-a subgroup of K+ channelopathies. Eur. J. Hum. Genet. 29, 1384–1395. https://doi.org/10.1038/s41431-021-00818-9.

Hock, J.M., Krishnan, V., Onyia, J.E., Bidwell, J.P., Milas, J., Stanislaus, D., 2001. Osteoblast apoptosis and bone turnover. J. Bone Miner. Res. 16, 975–984. https://doi.org/10.1359/jbmr.2001.16.6.975.

Hou, P.-S., Chuang, C.-Y., Kao, C.-F., Chou, S.-J., Stone, L., Ho, H.-N., Chien, C.-L., Kuo, H.-C., 2013. LHX2 regulates the neural differentiation of human embryonic stem cells via transcriptional modulation of PAX6 and CER1. Nucleic Acids Res. 41, 7753–7770. https://doi.org/10.1093/nar/gkt567.

Ianevski, A., Giri, A.K., Aittokallio, T., 2022. Fully-automated and ultra-fast cell-type identification using specific marker combinations from single-cell transcriptomic data. Nat. Commun. 13, 1246. https://doi.org/10.1038/s41467-022-28803-w.

Ivanovski, I., Djuric, O., Caraffi, S.G., Santodirocco, D., Pollazzon, M., Rosato, S., Cordelli, D.M., Abdalla, E., Accorsi, P., Adam, M.P., Ajmone, P.F., Badura-Stronka, M., Baldo, C., Baldi, M., Bayat, A., Bigoni, S., Bonvicini, F., Breckpot, J., Callewaert, B., Cocchi, G., Cuturilo, G., De Brasi, D., Devriendt, K., Dinulos, M.B., Hjortshøj, T.D., Epifanio, R., Faravelli, F., Fiumara, A., Formisano, D., Giordano, L., Grasso, M., Grønborg, S., Iodice, A., Iughetti, L., Kuburovic, V., Kutkowska-Kazmierczak, A., Lacombe, D., Lo Rizzo, C., Luchetti, A., Malbora, B., Mammi, I., Mari, F., Montorsi, G., Moutton, S., Møller, R.S., Muschke, P., Nielsen, J.E.K., Obersztyn, E., Pantaleoni, C., Pellicciari, A., Pisanti, M.A., Prpic, I., Poch-Olive, M.L., Raviglione, F., Renieri, A., Ricci, E., Rivieri, F., Santen, G.W., Savasta, S., Scarano, G., Schanze, I., Selicorni, A., Silengo, M., Smigiel, R., Spaccini, L., Sorge, G., Szczaluba, K., Tarani, L., Tone, L.G., Toutain, A., Trimouille, A., Valera, E.T., Vergano, S.S., Zanotta, N., Zenker, M., Conidi, A., Zollino, M., Rauch, A., Zweier, C., Garavelli, L., 2018. Phenotype and genotype of 87 patients with Mowat-Wilson

syndrome and recommendations for care. Genet. Med. 20, 965–975. https://doi.org/10.1038/gim.2017.221.
Keller, R.B., Tran, T.T., Pyott, S.M., Pepin, M.G., Savarirayan, R., McGillivray, G., Nickerson, D.A., Bamshad, M.J., Byers, P.H., 2018. Monoallelic and biallelic CREB3L1 variant causes mild and severe osteogenesis imperfecta, respectively. Genet. Med. 20, 411–419. https://doi.org/10.1038/gim.2017.115.
Kucukdereli, H., Allen, N.J., Lee, A.T., Feng, A., Ozlu, M.I., Conatser, L.M., Chakraborty, C., Workman, G., Weaver, M., Sage, E.H., Barres, B.A., Eroglu, C., 2011. Control of excitatory CNS synaptogenesis by astrocyte-secreted proteins Hevin and SPARC. Proc. Natl. Acad. Sci. USA 108, E440–E449. https://doi.org/10.1073/pnas.1104977108.
Liu, T., Li, T., Ke, S., 2023. Role of the CASZ1 transcription factor in tissue development and disease. Eur. J. Med. Res. 28, 562. https://doi.org/10.1186/s40001-023-01548-y.
Lories, R.J., Corr, M., Lane, N.E., 2013. To Wnt or not to Wnt: the bone and joint health dilemma. Nat. Rev. Rheumatol. 9, 328–339. https://doi.org/10.1038/nrrheum.2013.25.
Martins, H.C., Gilardi, C., Sungur, A.Ö., Winterer, J., Pelzl, M.A., Bicker, S., Gross, F., Kisko, T.M., Malikowska-Racia, N., Braun, M.D., Brosch, K., Nenadic, I., Stein, F., Meinert, S., Schwarting, R.K.W., Dannlowski, U., Kircher, T., Wöhr, M., Schratt, G., 2022. Bipolar-associated miR-499-5p controls neuroplasticity by downregulating the Cav1.2 subunit CACNB2. EMBO Rep. 23, e54420. https://doi.org/10.15252/embr.202154420.
Mayerl, S., Chen, J., Salveridou, E., Boelen, A., Darras, V.M., Heuer, H., 2022. Thyroid hormone transporter deficiency in mice impacts multiple stages of GABAergic interneuron development. Cereb. Cortex 32, 329–341. https://doi.org/10.1093/cercor/bhab211.
McKinsey, G.L., Lindtner, S., Trzcinski, B., Visel, A., Pennacchio, L.A., Huylebroeck, D., Higashi, Y., Rubenstein, J.L.R., 2013. Dlx1&2-dependent expression of Zfhx1b (Sip1, Zeb2) regulates the fate switch between cortical and striatal interneurons. Neuron 77, 83–98. https://doi.org/10.1016/j.neuron.2012.11.035.
Miyamoto, Y., Nagayoshi, I., Nishi, A., Fukuda, T., 2019. Three divisions of the mouse caudal striatum differ in the proportions of dopamine D1 and D2 receptor-expressing cells, distribution of dopaminergic axons, and composition of cholinergic and GABAergic interneurons. Brain Struct. Funct. 224, 2703–2716. https://doi.org/10.1007/s00429-019-01928-3.
Mouton-Liger, F., Thomas, S., Rattenbach, R., Magnol, L., Larigaldie, V., Ledru, A., Herault, Y., Verney, C., Créau, N., 2011. PCP4 (PEP19) overexpression induces premature neuronal differentiation associated with ca(2+) /calmodulin-dependent kinase II-δ activation in mouse models of down syndrome. J. Comp. Neurol. 519, 2779–2802. https://doi.org/10.1002/cne.22651.
Mowat, D.R., Croaker, G.D., Cass, D.T., Kerr, B.A., Chaitow, J., Adès, L.C., Chia, N.L., Wilson, M.J., 1998. Hirschsprung disease, microcephaly, mental retardation, and characteristic facial features: delineation of a new syndrome and identification of a locus at chromosome 2q22-q23. J. Med. Genet. 35, 617–623. https://doi.org/10.1136/jmg.35.8.617.
Mughal, A., O'Rourke, S.T., 2018. Vascular effects of apelin: mechanisms and therapeutic potential. Pharmacol. Ther. 190, 139–147. https://doi.org/10.1016/j.pharmthera.2018.05.013.
Mullins, N., Forstner, A.J., O'Connell, K.S., Coombes, B., Coleman, J.R.I., Qiao, Z., Als, T. D., Bigdeli, T.B., Børte, S., Bryois, J., Charney, A.W., Drange, O.K., Gandal, M.J., Hagenaars, S.P., Ikeda, M., Kamitaki, N., Kim, M., Krebs, K., Panagiotaropoulou, G., Schilder, B.M., Sloofman, L.G., Steinberg, S., Trubetskoy, V., Winsvold, B.S., Won, H.-H., Abramova, L., Adorjan, K., Agerbo, E., Al Eissa, M., Albani, D., Alliey-Rodriguez, N., Anjorin, A., Antilla, V., Antoniou, A., Awasthi, S., Baek, J.H., Bækvad-Hansen, M., Bass, N., Bauer, M., Beins, E.C., Bergen, S.E., Birner, A., Bøcker Pedersen, C., Bøen, E., Boks, M.P., Bosch, R., Brum, M., Brumpton, B.M., Brunkhorst-Kanaan, N., Budde, M., Bybjerg-Grauholm, J., Byerley, W., Cairns, M., Casas, M., Cervantes, P., Clarke, T.-K., Cruceanu, C., Cuellar-Barboza, A., Cunningham, J., Curtis, D., Czerski, P.M., Dale, A.M., Dalkner, N., David, F.S., Degenhardt, F., Djurovic, S., Dobbyn, A.L., Douzenis, A., Elvsåshagen, T., Escott-Price, V., Ferrier, I. N., Fiorentino, A., Foroud, T.M., Forty, L., Frank, J., Frei, O., Freimer, N.B., Frisén, L., Gade, K., Garnham, J., Gelernter, J., Giørtz Pedersen, M., Gizer, I.R., Gordon, S.D., Gordon-Smith, K., Greenwood, T.A., Grove, J., Guzman-Parra, J., Ha, K., Haraldsson, M., Hautzinger, M., Heilbronner, U., Hellgren, D., Herms, S., Hoffmann, P., Holmans, P.A., Huckins, L., Jamain, S., Johnson, J.S., Kalman, J.L., Kamatani, Y., Kennedy, J.L., Kittel-Schneider, S., Knowles, J.A., Kogevinas, M., Koromina, M., Kranz, T.M., Kranzler, H.R., Kubo, M., Kupka, R., Kushner, S.A., Lavebratt, C., Lawrence, J., Leber, M., Lee, H.-J., Lee, P.H., Levy, S.E., Lewis, C., Liao, C., Lucae, S., Lundberg, M., MacIntyre, D.J., Magnusson, S.H., Maier, W., Maihofer, A., Malaspina, D., Maratou, E., Martinsson, L., Mattheisen, M., McCarroll, S.A., McGregor, N.W., McGuffin, P., McKay, J.D., Medeiros, H., Medland, S.E., Millischer, V., Montgomery, G.W., Moran, J.L., Morris, D.W., Mühleisen, T.W., O'Brien, N., O'Donovan, C., Olde Loohuis, L.M., Oruc, L., Papiol, S., Pardiñas, A.F., Perry, A., Pfennig, A., Porichi, E., Potash, J.B., Quested, D., Raj, T., Rapaport, M.H., DePaulo, J.R., Regeer, E.J., Rice, J.P., Rivas, F., Rivera, M., Roth, J., Roussos, P., Ruderfer, D.M., Sánchez-Mora, C., Schulte, E.C., Senner, F., Sharp, S., Shilling, P.D., Sigurdsson, E., Sirignano, L., Slaney, C., Smeland, O.B., Smith, D.J., Sobell, J.L., Søholm Hansen, C., Soler Artigas, M., Spijker, A.T., Stein, D. J., Strauss, J.S., Świątkowska, B., Terao, C., Thorgeirsson, T.E., Toma, C., Tooney, P., Tsermpini, E.-E., Vawter, M.P., Vedder, H., Walters, J.T.R., Witt, S.H., Xi, S., Xu, W., Yang, J.M.K., Young, A.H., Young, H., Zandi, P.P., Zhou, H., Zillich, L., All-In Psychiatry, H.U.N.T., Adolfsson, R., Agartz, I., Alda, M., Alfredsson, L., Babadjanova, G., Backlund, L., Baune, B.T., Bellivier, F., Bengesser, S., Berrettini, W. H., Blackwood, D.H.R., Boehnke, M., Børglum, A.D., Breen, G., Carr, V.J., Catts, S., Corvin, A., Craddock, N., Dannlowski, U., Dikeos, D., Esko, T., Etain, B., Ferentinos, P., Frye, M., Fullerton, J.M., Gawlik, M., Gershon, E.S., Goes, F.S., Green, M.J., Grigoroiu-Serbanescu, M., Hauser, J., Henskens, F., Hillert, J., Hong, K. S., Hougaard, D.M., Hultman, C.M., Hveem, K., Iwata, N., Jablensky, A.V., Jones, I., Jones, L.A., Kahn, R.S., Kelsoe, J.R., Kirov, G., Landén, M., Leboyer, M., Lewis, C.M., Li, Q.S., Lissowska, J., Lochner, C., Loughland, C., Martin, N.G., Mathews, C.A., Mayoral, F., McElroy, S.L., McIntosh, A.M., McMahon, F.J., Melle, I., Michie, P., Milani, L., Mitchell, P.B., Morken, G., Mors, O., Mortensen, P.B., Mowry, B., Müller-Myhsok, B., Myers, R.M., Neale, B.M., Nievergelt, C.M., Nordentoft, M., Nöthen, M. M., O'Donovan, M.C., Oedegaard, K.J., Olsson, T., Owen, M.J., Paciga, S.A., Pantelis, C., Pato, C., Pato, M.T., Patrinos, G.P., Perlis, R.H., Posthuma, D., Ramos-Quiroga, J.A., Reif, A., Reininghaus, E.Z., Ribasés, M., Rietschel, M., Ripke, S., Rouleau, G.A., Saito, T., Schall, U., Schalling, M., Schofield, P.R., Schulze, T.G., Scott, L.J., Scott, R.J., Serretti, A., Shannon Weickert, C., Smoller, J.W., Stefansson, H., Stefansson, K., Stordal, E., Streit, F., Sullivan, P.F., Turecki, G., Vaaler, A.E., Vieta, E., Vincent, J.B., Waldman, I.D., Weickert, T.W., Werge, T., Wray, N.R., Zwart, J.-A., Biernacka, J.M., Nurnberger, J.I., Cichon, S., Edenberg, H. J., Stahl, E.A., McQuillin, A., Di Florio, A., Ophoff, R.A., Andreassen, O.A., 2021. Genome-wide association study of more than 40,000 bipolar disorder cases provides new insights into the underlying biology. Nat. Genet. 53, 817–829. https://doi.org/10.1038/s41588-021-00857-4.
Musante, I., Cangelosi, D., Muzzi, L., Jaudon, F., Di Duca, M., Guerrisi, S., Antonini, F., De Spelorzi, Y.C.C., Cingolani, L.A., Zara, F., Scudieri, P., 2025. CACNA1A loss-of-function affects neurogenesis in human iPSC-derived neural models. Cell. Mol. Life Sci. 82, 234. https://doi.org/10.1007/s00018-025-05740-7.
Ninfali, C., Siles, L., Esteve-Codina, A., Postigo, A., 2023. The mesodermal and myogenic specification of hESCs depend on ZEB1 and are inhibited by ZEB2. Cell Rep. 42, 113222. https://doi.org/10.1016/j.celrep.2023.113222.
Pfisterer, U., Petukhov, V., Demharter, S., Meichsner, J., Thompson, J.J., Batiuk, M.Y., Asenjo-Martinez, A., Vasistha, N.A., Thakur, A., Mikkelsen, J., Adorjan, I., Pinborg, L.H., Pers, T.H., von Engelhardt, J., Kharchenko, P.V., Khodosevich, K., 2020. Identification of epilepsy-associated neuronal subtypes and gene expression underlying epileptogenesis. Nat. Commun. 11, 5038. https://doi.org/10.1038/s41467-020-18752-7.
Ricci, E., Fetta, A., Garavelli, L., Caraffi, S., Ivanovski, I., Bonanni, P., Accorsi, P., Giordano, L., Pantaleoni, C., Romeo, A., Arena, A., Bonetti, S., Boni, A., Chiarello, D., Di Pisa, V., Epifanio, R., Faravelli, F., Finardi, E., Fiumara, A., Grioni, D., Mammi, I., Negrin, S., Osanni, E., Raviglione, F., Rivieri, F., Rizzi, R., Savasta, S., Tarani, L., Zanotta, N., Mowat Wilson Epilepsy Study Group, Dormi, A., Vignoli, A., Canevini, M., Cordelli, D.M., 2021. Further delineation and long-term evolution of electroclinical phenotype in Mowat Wilson syndrome. A longitudinal study in 40 individuals. Epilepsy Behav. 124, 108315. https://doi.org/10.1016/j.yebeh.2021.108315.
Schuster, J., Klar, J., Khalfallah, A., Laan, L., Hoeber, J., Fatima, A., Sequeira, V.M., Jin, Z., Korol, S.V., Huss, M., Nordgren, A., Anderlid, B.M., Gallant, C., Birnir, B., Dahl, N., 2022. ZEB2 haploinsufficient Mowat-Wilson syndrome induced pluripotent stem cells show disrupted GABAergic transcriptional regulation and function. Front. Mol. Neurosci. 15, 988993. https://doi.org/10.3389/fnmol.2022.988993.
Srivatsa, S., Parthasarathy, S., Molnár, Z., Tarabykin, V., 2015. Sip1 downstream effector ninein controls neocortical axonal growth, ipsilateral branching, and microtubule growth and stability. Neuron 85, 998–1012. https://doi.org/10.1016/j.neuron.2015.01.018.
St Peter, C., Hossain, W.A., Lovell, S., Rafi, S.K., Butler, M.G., 2024. Mowat-Wilson syndrome: case report and review of ZEB2 gene variant types, protein defects and molecular interactions. Int. J. Mol. Sci. 25, 2838. https://doi.org/10.3390/ijms25052838.
Takagi, T., Nishizaki, Y., Matsui, F., Wakamatsu, N., Higashi, Y., 2015. De novo inbred heterozygous Zeb2/Sip1 mutant mice uniquely generated by germ-line conditional knockout exhibit craniofacial, callosal and behavioral defects associated with Mowat-Wilson syndrome. Hum. Mol. Genet. 24, 6390–6402. https://doi.org/10.1093/hmg/ddv350.
Theocharis, A.D., Skandalis, S.S., Gialeli, C., Karamanos, N.K., 2016. Extracellular matrix structure. Adv. Drug Deliv. Rev. 97, 4–27. https://doi.org/10.1016/j.addr.2015.11.001.
Tiraboschi, E., Martina, S., van der Ent, W., Grzyb, K., Gawel, K., Cordero-Maldonado, M. L., Poovathingal, S.K., Heintz, S., Satheesh, S.V., Brattespe, J., Xu, J., Suster, M., Skupin, A., Esguerra, C.V., 2020. New insights into the early mechanisms of epileptogenesis in a zebrafish model of Dravet syndrome. Epilepsia 61, 549–560. https://doi.org/10.1111/epi.16456.
Tomassy, G.S., Lodato, S., Arlotta, P., 2013. A sip of GABA for the cerebral cortex. Neuron 77, 1–3. https://doi.org/10.1016/j.neuron.2012.12.026.
van den Berghe, V., Stappers, E., Vandesande, B., Dimidschstein, J., Kroes, R., Francis, A., Conidi, A., Lesage, F., Dries, R., Cazzola, S., Berx, G., Kessaris, N., Vanderhaeghen, P., van IJcken, W., Grosveld, F.G., Goossens, S., Haigh, J.J., Fishell, G., Goffinet, A., Aerts, S., Huylebroeck, D., Seuntjens, E., 2013. Directed migration of cortical interneurons depends on the cell-autonomous action of Sip1. Neuron 77, 70–82. https://doi.org/10.1016/j.neuron.2012.11.009.
Vandenbriele, C., Kauskot, A., Vandersmissen, I., Criel, M., Geenens, R., Craps, S., Luttun, A., Janssens, S., Hoylaerts, M.F., Verhamme, P., 2015. Platelet endothelial aggregation receptor-1: a novel modifier of neoangiogenesis. Cardiovasc. Res. 108, 124–138. https://doi.org/10.1093/cvr/cvv193.
Vandewalle, C., Comijn, J., De Craene, B., Vermassen, P., Bruyneel, E., Andersen, H., Tulchinsky, E., Van Roy, F., Berx, G., 2005. SIP1/ZEB2 induces EMT by repressing genes of different epithelial cell-cell junctions. Nucleic Acids Res. 33, 6566–6578. https://doi.org/10.1093/nar/gki965.
Yoo, Y., Jung, J., Lee, Y.-N., Lee, Y., Cho, H., Na, E., Hong, J., Kim, E., Lee, Jin Sook, Lee, Je Sang, Hong, C., Park, S.-Y., Wie, J., Miller, K., Shur, N., Clow, C., Ebel, R.S.,

DeBrosse, S.D., Henderson, L.B., Willaert, R., Castaldi, C., Tikhonova, I., Bilgüvar, K., Mane, S., Kim, K.J., Hwang, Y.S., Lee, S.-G., So, I., Lim, B.C., Choi, H.-J., Seong, J.Y., Shin, Y.B., Jung, H., Chae, J.-H., Choi, M., 2017. GABBR2 mutations determine phenotype in rett syndrome and epileptic encephalopathy. Ann. Neurol. 82, 466–478. https://doi.org/10.1002/ana.25032.